eLIFE elifesciences.org

TOOLS AND RESOURCES

Functional proteomic atlas of HIV infection in primary human CD4+ T cells

Adi Naamati[1], James C Williamson[1,2], Edward JD Greenwood[1,2], Sara Marelli[1], Paul J Lehner[2], Nicholas J Matheson[1]*

[1]Department of Medicine, University of Cambridge, Cambridge, United Kingdom; [2]Cambridge Institute for Medical Research, University of Cambridge, Cambridge, United Kingdom

Abstract Viruses manipulate host cells to enhance their replication, and the identification of cellular factors targeted by viruses has led to key insights into both viral pathogenesis and cell biology. In this study, we develop an HIV reporter virus (HIV-AFMACS) displaying a streptavidin-binding affinity tag at the surface of infected cells, allowing facile one-step selection with streptavidin-conjugated magnetic beads. We use this system to obtain pure populations of HIV-infected primary human CD4+ T cells for detailed proteomic analysis, and quantitate approximately 9000 proteins across multiple donors on a dynamic background of T cell activation. Amongst 650 HIV-dependent changes ($q < 0.05$), we describe novel Vif-dependent targets FMR1 and DPH7, and 192 proteins not identified and/or regulated in T cell lines, such as ARID5A and PTPN22. We therefore provide a high-coverage functional proteomic atlas of HIV infection, and a mechanistic account of host factors subverted by the virus in its natural target cell.

DOI: https://doi.org/10.7554/eLife.41431.001

***For correspondence:** njm25@cam.ac.uk

Competing interests: The authors declare that no competing interests exist.

Funding: See page 21

Received: 31 August 2018
Accepted: 10 February 2019
Published: 12 March 2019

Reviewing editor: Jeremy Luban, University of Massachusetts Medical School, United States

Introduction

Remodelling of the host proteome during viral infection may reflect direct effects of viral proteins, secondary effects or cytopathicity accompanying viral replication, or host countermeasures such as the interferon (IFN) response. By defining time-dependent changes in protein levels in infected cells, and correlating temporal profiles of cellular and viral proteins, we have shown that it is possible to differentiate these phenomena, and identify direct cellular targets of human cytomegalovirus (HCMV) and HIV (***Greenwood et al., 2016***; ***Matheson et al., 2015***; ***Weekes et al., 2014***). To enable time course analysis and minimise confounding effects from uninfected bystander cells, pure populations of synchronously infected cells must be sampled sequentially as they progress through a single round of viral replication. In the case of HIV, we previously satisfied these conditions by spinoculating the highly permissive CEM-T4 lymphoblastoid T cell line (***Foley et al., 1965***; ***O'Doherty et al., 2000***; ***Popovic et al., 1984***) with Env-deficient NL4-3-ΔEnv-EGFP virus (***Zhang et al., 2004***) at a high multiplicity of infection (MOI) (***Greenwood et al., 2016***).

The utility of cancer cell line models (such as CEM-T4) is, however, limited by the extent to which they retain the characteristics of the primary cells from which they were derived, and cancer-specific and *in vitro* culture-dependent reprogramming are well described (***Gillet et al., 2013***). For example, the HIV accessory proteins Vif, Nef and Vpu are required for viral replication in primary T cells, but not in many T cell lines (***Neil et al., 2008***; ***Rosa et al., 2015***; ***Sheehy et al., 2002***; ***Usami et al., 2015***), and HIV is restricted by type I IFN in primary T cells, but not CEM-derived T cells (***Goujon et al., 2013***). In addition, whilst ensuring a high % infection, dysregulation of the cellular proteome at high MOIs may not be indicative of protein changes when a single transcriptionally active provirus is present per cell.

In this study, we therefore sought to apply our temporal proteomic approach to HIV infection of primary human CD4+ T lymphocytes, the principle cell type infected *in vivo*, at an MOI $\leq$ 1. To this end, we have developed an HIV reporter virus encoding a cell surface streptavidin-binding affinity tag, allowing antibody-free magnetic cell sorting of infected cells (AFMACS) (***Matheson et al., 2014***) (***Figure 1A***). This system allows rapid, scalable, affinity purification of HIV-infected cells from mixed cultures, bypassing the need for high MOIs or fluorescence-activated cell sorting (FACS). We use this system to generate a detailed atlas of cellular protein dynamics in HIV-infected primary human CD4+ T cells, show how this resource can be used to identify novel cellular proteins regulated by HIV, and assign causality to individual HIV accessory proteins.

Results

Design and construction of the HIV-AFMACS reporter virus

AFMACS-based magnetic selection requires the high-affinity 38 amino acid streptavidin-binding peptide (SBP) (***Keefe et al., 2001***) to be displayed at the cell surface by fusion to the N-terminus of the truncated Low-affinity Nerve Growth Factor Receptor (SBP-ΔLNGFR) (***Ruggieri et al., 1997***). Cells expressing this marker may be selected directly with streptavidin-conjugated magnetic beads, washed to remove unbound cells, then released by incubation with the naturally occurring vitamin biotin (***Matheson et al., 2014***). To engineer a single round HIV reporter virus encoding SBP-ΔLNGFR, we considered three settings in the proviral construct: fused to the endogenous Env signal peptide (as a direct replacement for Env); or as an additional cistron, downstream of *nef* and either a P2A peptide or IRES. We used Env-deficient pNL4-3-ΔEnv-EGFP (HIV-1) as a backbone and, since increased size of lentiviral genome is known to reduce packaging efficiency (***Kumar et al., 2001***), tested each approach in constructs from which EGFP was removed and/or the 3' long terminal repeat (LTR) truncated. Further details relating to construct design are described in the Materials and methods and ***Supplementary file 1***.

For initial screening, VSVg-pseudotyped viruses were made in HEK-293T cells under standard conditions, and used to spinoculate CEM-T4 T cells (CEM-T4s). Infected cells were identified by expression of EGFP and/or cell surface LNGFR, combined with Nef/Vpu-mediated downregulation of CD4 (***Guy et al., 1987***; ***Willey et al., 1992***). Whilst infection is not truly 'productive' (because Env is deleted), Gag alone is sufficient for assembly and release of virions (***Gheysen et al., 1989***), and other structural and non-structural viral proteins are expressed in accordance with full length viral infection (***Greenwood et al., 2016***).

As expected, all viruses tested expressed SBP-ΔLNGFR at the cell surface of infected cells (***Figure 1—figure supplement 1A***), but the larger constructs resulted in lower infectious viral titres (***Figure 1—figure supplement 1A–B***). We therefore selected pNL4-3-ΔEnv-SBP-ΔLNGFR, pNL4-3-ΔENV-Nef-P2A-SBP-ΔLNGFR and pNL4-3-ΔEnv-Nef-IRES-SBP-ΔLNGFR-Δ3 for further evaluation (***Figure 1—figure supplement 2***). Viruses generated from these constructs expressed high levels of SBP-ΔLNGFR 48 hr post-infection, and depleted CD4 and tetherin to a similar extent. However, only the pNL4-3-ΔENV-Nef-P2A-SBP-ΔLNGFR virus (***Figure 1B***) expressed high levels of LNGFR 24 hr post-infection in both CEM-T4s (***Figure 1—figure supplement 2***) and primary human CD4+ T cells (***Figure 1C***). This is consistent with Nef-P2A-SBP-ΔLNGFR expression from completely spliced transcripts early in HIV infection (***Klotman et al., 1991***), with the P2A peptide ensuring that translation of Nef and SBP-ΔLNGFR follow similar kinetics.

Since analysis of cells at early as well as late time points is essential for the generation of time course data, we focussed on pNL4-3-ΔEnv-Nef-P2A-SBP-ΔLNGFR (now termed HIV-AFMACS). To confirm that HIV-AFMACS virus could be used for cell selection (***Figure 1A***), infected primary T cells were captured by streptavidin-conjugated magnetic beads, released by incubation with excess biotin, then analysed by flow cytometry. Compared with unselected cells (input) or cells released during washing (flow-through), selected cells were markedly enriched for SBP-ΔLNGFR expression and CD4 downregulation (***Figure 1D***). In fact, from mixed populations containing approximately 20–40% infected cells, purities of $\geq$ 90% were routinely achieved by AFMACS of both CEM-T4s and primary human CD4+ T cells, with $\leq$ 10% infected cells lost in the flow-through (***Figure 1E***). The full HIV-

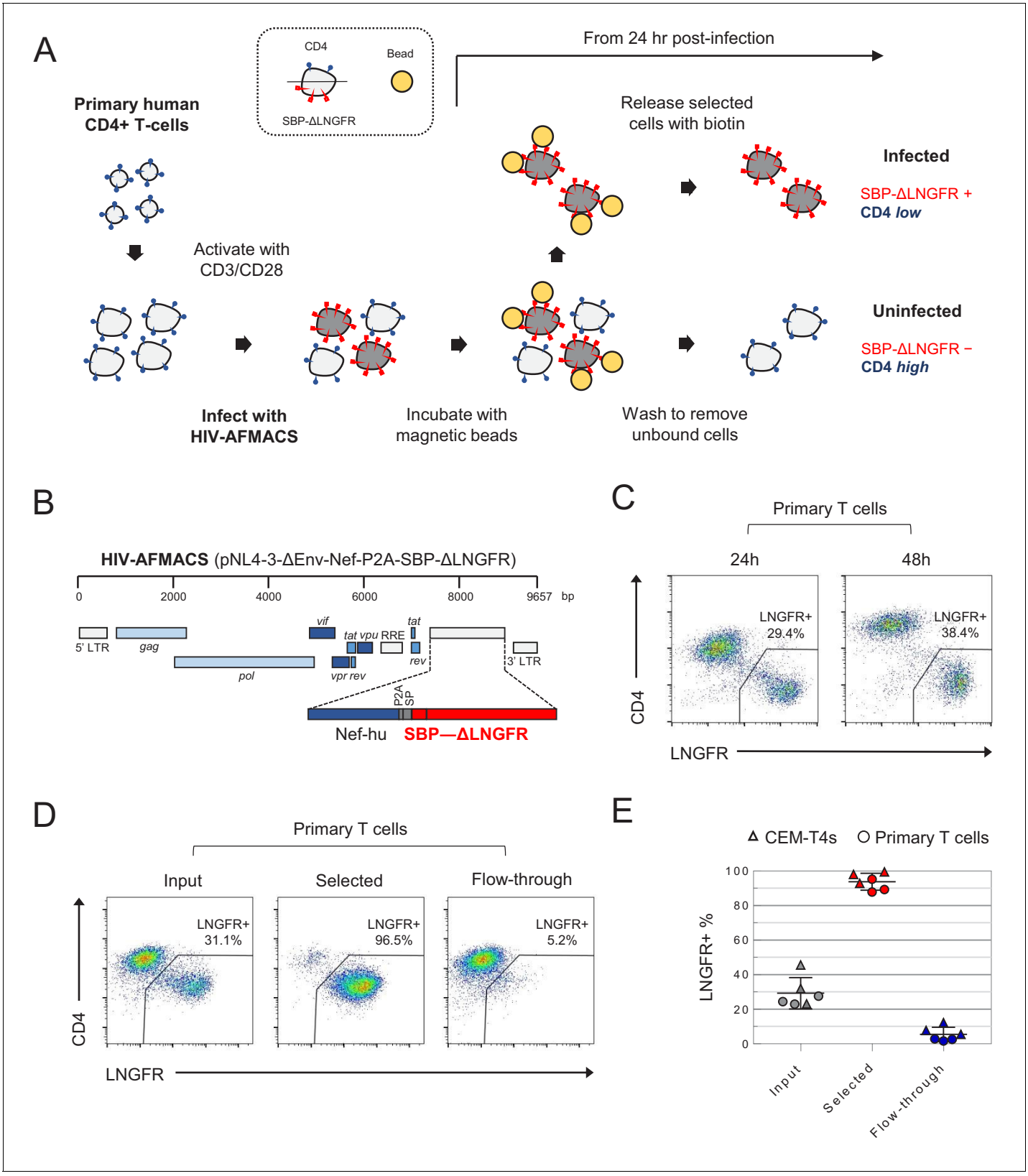

Figure 1. Antibody-free magnetic selection of HIV-infected primary T cells. (**A**) Workflow for AFMACS-based magnetic selection of HIV-infected primary T cells. (**B**) Schematic of HIV-AFMACS provirus (pNL4-3-ΔEnv-Nef-P2A-SBP-ΔLNGFR). For simplicity, reading frames are drawn to match the HXB2 HIV-1 reference genome. Length is indicated in base pairs (bp). The complete sequence is available in ***Supplementary file 1***. Nef-hu, codon-optimised Nef;

Figure 1 continued on next page

Figure 1 continued

RRE, Rev response element; SP, signal peptide. (**C**) Expression of cell surface SBP-ΔLNGFR and CD4 on primary T cells 24 or 48 hr post-infection with HIV-AFMACS. Cells were stained with anti-LNGFR and anti-CD4 antibodies at the indicated time points and analysed by flow cytometry. (**D–E**) Magnetic sorting of HIV-infected (red, LNGFR+, CD4 low) and uninfected (blue, LNGFR-, CD4 high) cells. Cells were separated using AFMACS 48 hr post-infection with HIV-AFMACS and analysed as in (**C**). Representative (**D**) and summary (**E**) data from six independent experiments in CEM-T4s (triangles) and primary T cells (circles) are shown, with means and 95% confidence intervals (CIs).

DOI: https://doi.org/10.7554/eLife.41431.002

The following figure supplements are available for figure 1:

Figure supplement 1. Initial screen of SBP-ΔLNGFR-expressing HIV viruses.

DOI: https://doi.org/10.7554/eLife.41431.003

Figure supplement 2. Time course evaluation of selected SBP-ΔLNGFR-expressing HIV viruses.

DOI: https://doi.org/10.7554/eLife.41431.004

AFMACS sequence is available from GenBank (accession: MK435310) and in ***Supplementary file 1***, and the proviral construct will be made available to the community via the National Institutes of Health (NIH) AIDS Reagent Program.

Time-dependent proteomic remodelling during HIV infection of primary T cells

To gain a comprehensive, unbiased overview of viral and cellular protein dynamics during HIV-infection of its natural target cell, we used the HIV-AFMACS virus to spinoculate activated, primary human CD4+ T cells, sorted infected (SBP-ΔLNGFR positive) and uninfected (SBP-ΔLNGFR negative) cells by AFMACS 24 hr and 48 hr post-infection, and analysed whole cell lysates using tandem mass tag (TMT)-based quantitative proteomics (***Figure 2A–B*** and ***Figure 2—figure supplement 1A***) (***Greenwood et al., 2016***; ***Weekes et al., 2014***). Interpretation of HIV-dependent proteomic remodelling in primary T cells is complicated by concurrent changes in relative protein abundance resulting from T cell activation (***Geiger et al., 2016***). We therefore exploited multiplex TMT labelling to measure parallel protein abundances in resting and activated (uninfected) T cells from the same donor, as well as control (mock-infected) T cells obtained at each time point.

In total, we quantitated 9070 cellular proteins across 10 different conditions. As previously reported (***Geiger et al., 2016***), T cell activation itself caused extensive proteomic remodelling, with relative abundances of 2677/9070 (29%) proteins changing by > 2 fold in activated vs resting cells (***Figure 2—figure supplement 2***). All data from infected and uninfected cells have been made available via ProteomeXchange with identifier PXD012263, and are summarised in an interactive spreadsheet allowing generation of temporal profiles for any quantitated proteins of interest (***Figure 2—source data 1***). For example, the restriction factor tetherin (targeted by HIV-1 Vpu [***Neil et al., 2008***]) is upregulated by T cell activation, then progressively depleted in HIV-infected (red, SBP-ΔLNGFR positive) but not uninfected (blue, SBP-ΔLNGFR negative) cells (***Figure 2C***, left panel). Conversely, the restriction factor SAMHD1 (targeted by some HIV-2/SIV Vpx and Vpr variants, but not HIV-1 [***Hrecka et al., 2011***; ***Laguette et al., 2011***; ***Lim et al., 2012***]) is depleted by T cell activation, independent of HIV infection (***Figure 2C***, right panel). In these graphical representations, relative protein abundances for each condition are depicted by bars, and ratios of protein abundances in paired experimental/control cells from each condition/time point are depicted by lines (grey, resting/activated; red, SBP-ΔLNGFR positive, infected; blue, SBP-ΔLNGFR negative, uninfected).

Aside from tetherin, levels of many other reported Vpu (CD4, SNAT1) (***Matheson et al., 2015***; ***Willey et al., 1992***), Nef (CD4, SERINC5) (***Guy et al., 1987***; ***Rosa et al., 2015***; ***Usami et al., 2015***), Vif (APOBEC3 and PPP2R5 families) (***Greenwood et al., 2016***; ***Sheehy et al., 2002***) and Vpr (UNG, HLTF, ZGPAT, VPRBP, MUS81, EME1, MCM10, TET2) (***Hrecka et al., 2016***; ***Lahouassa et al., 2016***; ***Lapek et al., 2017***; ***Lv et al., 2018***; ***Maudet et al., 2013***; ***Romani et al., 2015***; ***Schröfelbauer et al., 2005***; ***Zhou et al., 2016***) substrates were all reduced by HIV infection in primary T cells (***Figure 2D***, and ***Figure 2—figure supplement 1B***). Conversely, and consistent with our previous observations in CEM-T4s, APOBEC3B and SERINC1 were not depleted (***Figure 2—figure supplement 1B***) (***Greenwood et al., 2016***; ***Matheson et al., 2015***). In the absence of donor haplotyping, polymorphisms at the MHC-I locus make routine proteomic quantification problematic.

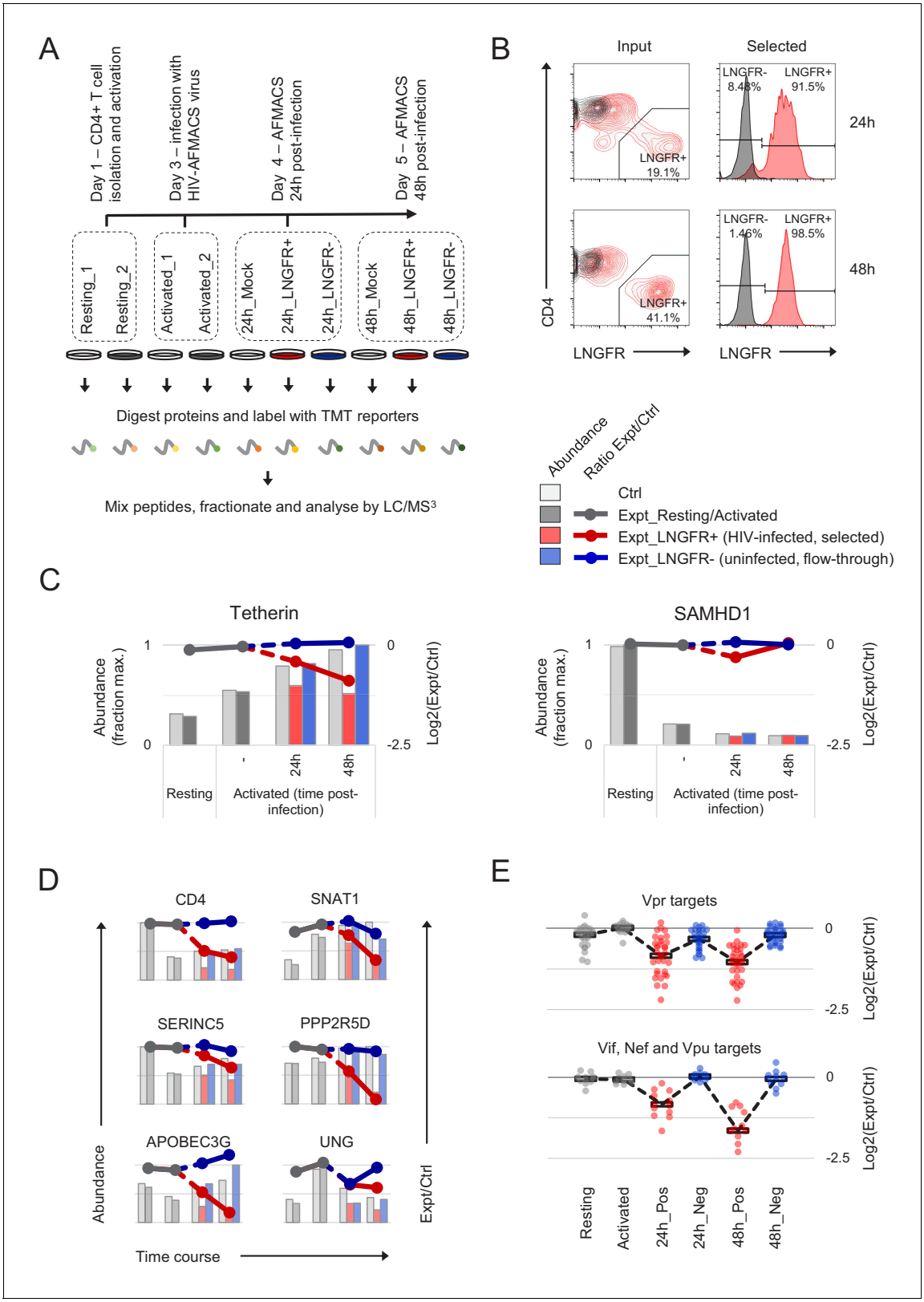

Figure 2. Temporal proteomic analysis of HIV infection in primary T cells. (**A**) Overview of time course proteomic experiment. Control (pale grey, resting/activated/mock) and experimental (dark grey, resting/activated; red, LNGFR+, HIV-infected, selected; blue, LNGFR-, uninfected, flow-through) cells are indicated for each condition/time point. (**B**) Magnetic sorting of HIV-infected (red, LNGFR+, selected) cells used for (**A**). Corresponding uninfected (LNGFR-, flow-through) cells are shown in ***Figure 2—figure supplement 1A***. Cells were separated using AFMACS at the indicated time

Figure 2 continued on next page

Figure 2 continued

points post-infection with HIV-AFMACS, stained with anti-LNGFR and anti-CD4 antibodies and analysed by flow cytometry. Mock-infected cells are shown in grey. (**C**) Expression profiles of illustrative restriction factors regulated by T cell activation and HIV infection (tetherin) or T cell activation alone (SAMHD1) in cells from (**A–B**). Relative abundances (bars, fraction of maximum) and log2(ratio)s of abundances (lines) in experimental (Expt):control (Ctrl) cells are shown for each condition/time point and coloured as in (**A**) (summarised in the key). (**D**) Expression profiles of illustrative accessory protein targets (CD4, Nef/Vpu; SERINC5, Nef; SNAT1, Vpu; APOBEC3G, Vif; PPP2R5D, Vif; UNG, Vpr) in cells from (**A–B**). Axes, scales and colours are as in (**C**). Expression profiles of other accessory protein targets are shown in ***Figure 2—figure supplement 1B***. (**E**) Patterns of temporal regulation of Vpr vs other accessory protein (Vif/Nef/Vpu) targets in cells from (**A–B**). Log2(ratio)s of abundances in experimental (Expt):control (Ctrl) cells are shown for 45 accessory protein targets (as in ***Figure 2—figure supplement 3A***). Colours are as in (**C**), and average profiles (mean, black lozenges/dotted lines) are highlighted for each group of targets.

DOI: https://doi.org/10.7554/eLife.41431.005

The following source data and figure supplements are available for figure 2:

Source data 1. Functional proteomic atlas of HIV-infection in primary human CD4+ T cells.

DOI: https://doi.org/10.7554/eLife.41431.006

Figure supplement 1. Additional controls for time course proteomic experiment.

DOI: https://doi.org/10.7554/eLife.41431.007

Figure supplement 2. Comparison with T cell activation-dependent changes in ***Geiger et al. (2016)***.

DOI: https://doi.org/10.7554/eLife.41431.008

Figure supplement 3. Temporal clustering of HIV accessory protein targets.

DOI: https://doi.org/10.7554/eLife.41431.009

Nonetheless, our data are consistent with depletion of HLA-A and HLA-B, but not HLA-C (***Figure 2—figure supplement 1B***), as previously reported for Nef/Vpu variants from NL4-3 HIV (***Apps et al., 2016***; ***Cohen et al., 1999***; ***Schwartz et al., 1996***).

Together with cellular proteins, we identified gene products from seven viral open reading frames (ORFs; ***Figure 2—figure supplement 1C***). As expected (***Karn and Stoltzfus, 2012***), viral regulatory and accessory proteins expressed from fully spliced, Rev-independent transcripts (Tat, Rev, Nef-P2A and SBP-ΔLNGFR) were expressed early in infection, peaking at 24 hr. Conversely, viral structural proteins expressed from unspliced, Rev-dependent transcripts (Gag and Gagpol) were expressed late in infection, increasing progressively from 24 to 48 hr. Viral accessory proteins expressed from partially spliced transcripts were either not detected (Vpr and Vpu) or incompletely quantitated (Vif).

Proteins and pathways regulated by HIV in primary T cells from multiple donors

Inter-individual variability is known to affect gene expression during T cell activation (***Ye et al., 2014***). Accordingly, to identify reproducible HIV targets, we analysed primary human CD4+ T cells from three further donors. In each case, mock-infected cells were compared with HIV-infected cells selected using AFMACS 48 hr post-infection (***Figure 3A–B*** and ***Figure 3—figure supplement 1A***). Aside from APOBEC3 proteins, we recently discovered the PPP2R5A-E (B56) family of PP2A phosphatase regulatory subunits to be degraded by diverse Vif variants, spanning primate and ruminant lentiviruses (***Greenwood et al., 2016***). To formally document Vif-dependent changes in primary T cells, both wildtype (WT) and Vif-deficient (ΔVif) viruses were therefore included. Whilst some donor-dependent differences were apparent, most sample-sample variability was accounted for by HIV infection (***Figure 3—figure supplement 1B***), and all accessory protein substrates from ***Figure 2C–D*** and ***Figure 2—figure supplement 1B*** were significantly depleted by WT HIV (***Figure 3C***, left panel). In total, we quantitated 8789 cellular proteins across nine different conditions, of which 650 were significantly regulated by HIV infection ($q < 0.05$) and are summarised in an interactive filter table (***Figure 3—source data 1***).

Compared with a previous, similar experiment using CEM-T4s (***Greenwood et al., 2016***), we observed greater variability in protein abundances between replicates (***Figure 3—figure supplement 2A***), but a high degree of correlation in HIV-dependent changes between cell types (***Figure 3—figure supplement 2B***). As well as 'canonical' accessory protein targets, we have recently discovered that most protein-level changes in HIV-infected CEM-T4s may be explained by primary and secondary effects of Vpr, including degradation of at least 34 additional substrates (***Greenwood et al., 2019***). These changes were recapitulated in primary T cells (***Figure 3C***, middle

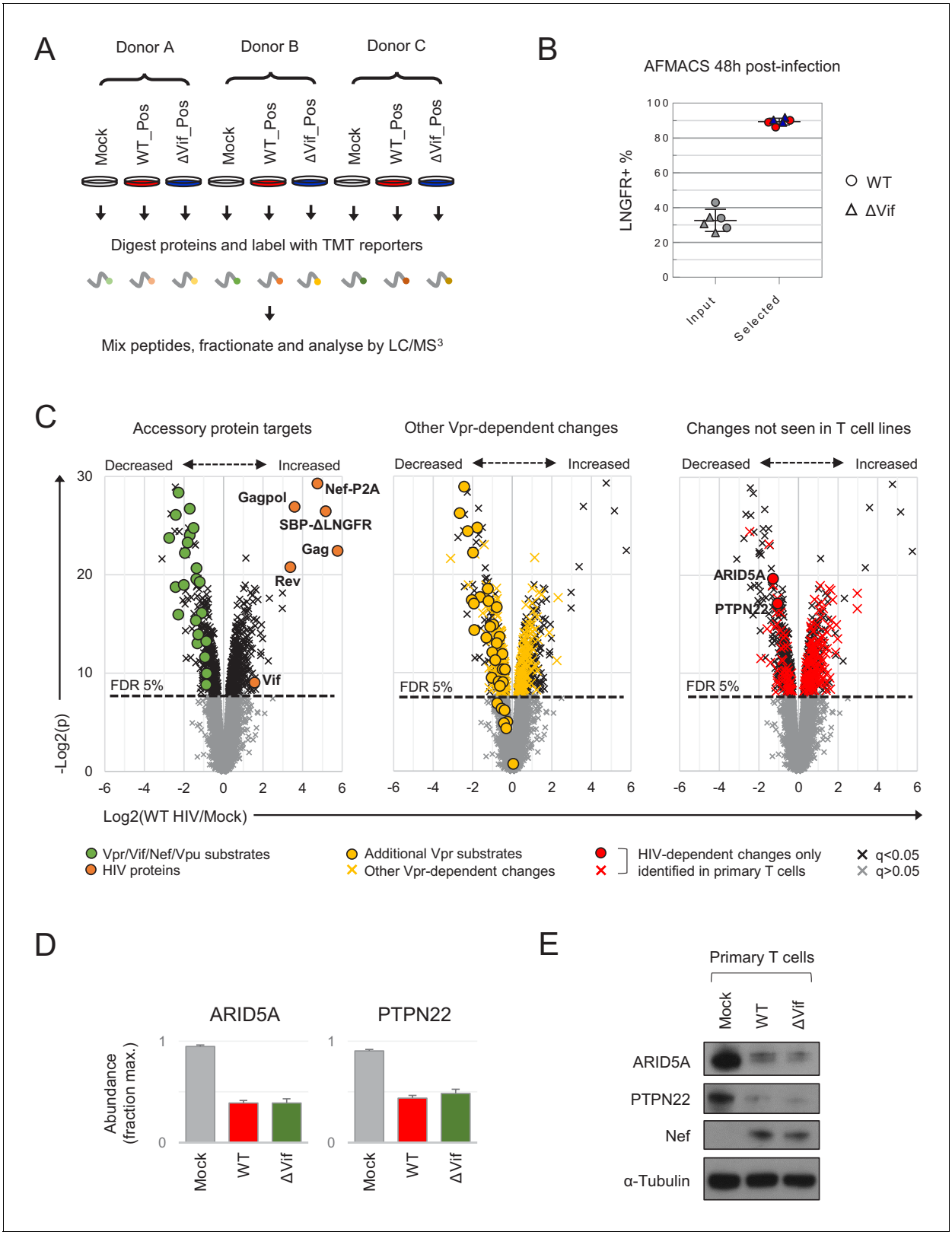

Figure 3. Proteins regulated by HIV in primary T cells. (**A**) Overview of single time point proteomic experiment. HIV-infected (LNGFR+) primary T cells were isolated using AFMACS 48 hr post-infection with WT (red) or ΔVif (blue) HIV-AFMACS. (**B**) AFMACS-based enrichment of WT (red circles) and ΔVif (blue triangles) HIV-infected (LNGFR+) cells used for (**A**), with means and 95% CIs. Corresponding cells pre-selection are included for each donor/virus (WT, grey circles; ΔVif, grey triangles). Cells were stained with anti-LNGFR and anti-CD4 antibodies and analysed by flow cytometry, with representative

Figure 3 continued on next page

Figure 3 continued

data in ***Figure 3—figure supplement 1A***. (**C**) Protein abundances in WT HIV-infected vs mock-infected cells from (**A**). Volcano plots show statistical significance (y axis) vs fold change (x axis) for 8789 cellular and six viral proteins quantitated in cells from all three donors (no missing values). Proteins with Benjamini-Hochberg FDR-adjusted p values (q values) < 0.05 or > 0.05 are indicated (FDR threshold of 5%). Proteins highlighted in each plot are summarised in the key. Vpr/Vif/Nef/Vpu substrates (green circles) comprise proteins from ***Figure 2C–D*** and ***Figure 2—figure supplement 1B***, excluding negative controls (SAMHD1, APOBEC3B, SERINC1, HLA-C) and HLA-A/B alleles (different in each donor) but including SMUG1 (not identified in time course proteomic experiment) (***Schröfelbauer et al., 2005***) and both quantitated isoforms of PP2R5C (Q13362 and Q13362-4) and ZGPAT (Q8N5A5 and Q8N5A5-2). Additional Vpr substrates (gold circles) and Vpr-dependent changes (gold crosses) comprise recently described direct and indirect Vpr targets (***Greenwood et al., 2019***). HIV-dependent changes only identified in primary T cells (red circles and crosses) comprise proteins with q < 0.05 either not identified or not concordantly regulated by HIV in CEM-T4s (***Greenwood et al., 2016***) (and exclude known accessory protein-dependent changes). Further details on comparator datasets used in this figure are provided in the Materials and methods. (**D–E**) Abundances of ARID5A and PTPN22 in mock-infected (grey), WT HIV-infected (red) and ΔVif HIV-infected (green) primary T cells from (**A**). Mean abundances (fraction of maximum) with 95% CIs are shown (**D**). As well as proteomic analysis, cells from donor A were lysed in 2% SDS and analysed by immunoblot with anti-ARID5A, anti-PTPN22, anti-Nef and anti-α-tubulin antibodies (**E**). Same lysates as ***Figure 5D***.

DOI: https://doi.org/10.7554/eLife.41431.010

The following source data and figure supplements are available for figure 3:

Source data 1. Proteins regulated by HIV and/or control lentivectors.

DOI: https://doi.org/10.7554/eLife.41431.011

Figure supplement 1. Additional controls for single time point proteomic experiment.

DOI: https://doi.org/10.7554/eLife.41431.012

Figure supplement 2. Comparison with HIV-dependent changes in CEM-T4s.

DOI: https://doi.org/10.7554/eLife.41431.013

Figure supplement 3. Comparison with HIV-dependent changes in other datasets.

DOI: https://doi.org/10.7554/eLife.41431.014

Figure supplement 4. Proteins regulated by transduction with control lentivectors.

DOI: https://doi.org/10.7554/eLife.41431.015

Figure supplement 5. Comparison with HIV-dependent changes in ***Kuo et al. (2018)***.

DOI: https://doi.org/10.7554/eLife.41431.016

panel), with 33 newly described Vpr substrates quantitated, and 32 decreased in abundance. Several other cell surface proteins reported to be downregulated by Nef and/or Vpu were also depleted, but the magnitude of effect was typically modest, and many were unchanged (***Figure 3—figure supplement 3A***, left panel). Likewise, we did not see evidence of HIV/Vif-dependent transcriptional regulation of RUNX1 target gene products such as T-bet/TBX21 (***Figure 3—figure supplement 3A***, middle panel) (***Kim et al., 2013***). Nonetheless, taken together, known accessory protein-dependent changes, characterised in transformed T cell lines, are able to account for 297/650 (46%) of proteins regulated by HIV in primary T cells (***Figure 3—figure supplement 3B***), including 175/299 (59%) of proteins decreased in abundance.

As with individual proteins, pathways and processes downregulated by HIV infection of primary T cells are dominated by the effects of accessory proteins (***Figure 4A–B***). These include the DNA damage response and cell cycle (Vpr) (***Greenwood et al., 2019***; ***He et al., 1995***; ***Jowett et al., 1995***; ***Laguette et al., 2014***; ***Poon et al., 1997***; ***Re et al., 1995***; ***Rogel et al., 1995***; ***Roshal et al., 2003***), cytidine deamination and PP2A activity (Vif) (***Greenwood et al., 2016***; ***Harris et al., 2003***; ***Sheehy et al., 2002***) and amino acid transport (Vpu/Nef) (***Matheson et al., 2015***). Proteins upregulated by HIV are more diverse, with fewer dominant functional clusters. Nonetheless, we saw marked increases in proteins associated with lipid and sterol metabolism (***Figure 4B–C***). A similar effect has been reported in T cell lines at the transcriptional level, and attributed to the expression of Nef (***Shrivastava et al., 2016***; ***van 't Wout et al., 2005***). Similarly, several proteins in these pathways are indirectly regulated by Vpr (***Figure 4C***) (***Greenwood et al., 2019***).

Identification and characterisation of primary T cell-specific HIV targets

Despite the overall agreement with cell line data, 1252/8789 (14%) cellular proteins quantitated here were not identified in a previous, similar experiment using CEM-T4s (***Greenwood et al., 2016***). Furthermore, having excluded known accessory-protein dependent changes, 192/650 (30%) proteins regulated by HIV in primary T cells were either not detected, or not significantly/concordantly regulated, in CEM-T4s (***Figure 3C***, right panel and ***Figure 3—figure supplement 3B***). These proteins

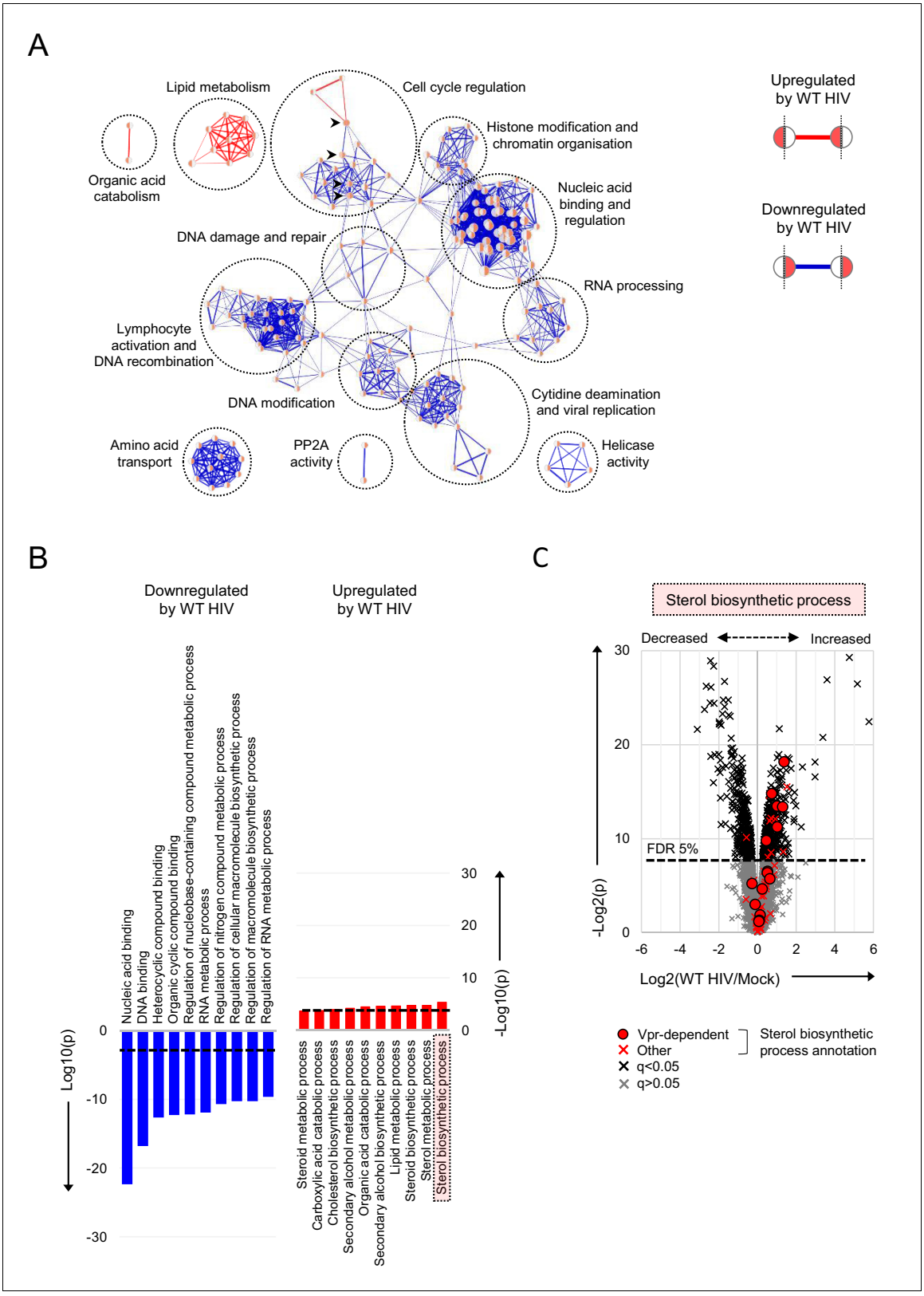

Figure 4. Pathways regulated by HIV in primary T cells. (**A–B**) Gene Ontology (GO) functional annotation terms enriched amongst upregulated or downregulated proteins with q < 0.05 in WT HIV-infected vs mock-infected cells from single time point proteomic experiment (***Figure 3A***). In the Enrichment Map (***Merico et al., 2010***) network-based visualisation (**A**), each node represents a GO term, with node size indicating number of annotated proteins, edge thickness representing degree of overlap (red, enriched amongst upregulated proteins; blue, enriched amongst

Figure 4 continued on next page

Figure 4 continued

downregulated proteins) and similar GO terms placed close together. Degree of enrichment is mapped to node colour (left side, enriched amongst upregulated proteins; right side, enriched amongst downregulated proteins) as a gradient from white (no enrichment) to red (high enrichment). Highlighted nodes (arrow heads) represent GO terms enriched amongst both upregulated and downregulated proteins. In the bar charts (**B**), the 10 most enriched GO terms (ranked by p value) amongst upregulated (red) and downregulated (blue) proteins are shown, with an indicative Benjamini-Hochberg FDR threshold of 5% (dashed line). (**C**) Protein abundances in WT HIV-infected vs mock-infected cells from single time point proteomic experiment (***Figure 3A***), with details for volcano plot as in ***Figure 3C***. 57 proteins annotated with the GO term 'sterol biosynthetic process' (GO:0016126) are highlighted in red. Amongst these, 15 proteins are regulated by Vpr in CEM-T4s (circles) (***Greenwood et al., 2019***).

DOI: https://doi.org/10.7554/eLife.41431.017

may represent accessory protein substrates expressed in primary T cells but not T cell lines, or proteins regulated by alternative, cell type-specific mechanisms, such as the interferon response (***Figure 3—figure supplement 3A***, right panel) (***Vermeire et al., 2016***).

We have previously shown that expression of the SBP-ΔLNGFR selectable marker as a transgene does not impact the viability, activation or proliferation of primary T cells (***Matheson et al., 2014***). Nonetheless, some of the novel changes attributed to HIV in this study could theoretically be secondary to exposure to VSVg-pseudotyped viral particles, expression of SBP-ΔLNGFR and/or the AFMACS workflow, or reflect pre-existing proteomic differences in infected (permissive) cells, compared with the mock-infected bulk population. To exclude these possibilities, we repeated the single time point proteomic experiment using primary T cells from three new donors and substituting WT and Vif-deficient HIV-AFMACS for two different control lentivectors expressing SBP-ΔLNGFR either as a single transgene (from the SFFV promoter; pSBP-ΔLNGFR) or in conjunction with HIV-1 Tat (from the HIV-1 LTR; pTat/SBP-ΔLNGFR) (***Figure 3—figure supplement 4A–C***).

As expected, changes in transduced cells were far less extensive than changes induced by HIV (***Figure 3—figure supplement 4D***, top and middle panels; compare with ***Figure 3C***). In fact, amongst 8518 cellular proteins quantitated across nine different conditions, only 37/8518 (0.4%) were significantly perturbed by one or both lentivectors ($q < 0.05$), and are summarised in an interactive filter table (***Figure 3—source data 1***). Interestingly, despite evidence of robust transactivation of the HIV LTR (resulting in high level expression of SBP-ΔLNGFR at the surface of cells transduced with pTat/SBP-ΔLNGFR), no Tat-dependent changes in cellular protein levels were identified (***Figure 3—figure supplement 4C***, lower panels and ***Figure 3—figure supplement 4D***, bottom panel). Most importantly, amongst the 650 proteins significantly regulated by HIV, 576 were quantitated in the SBP-ΔLNGFR control experiment, of which only one protein (MYB) was also significantly regulated by the control lentivectors (***Figure 3—figure supplement 4D***, top and middle panels and ***Figure 3—source data 1***).

To further validate our proteomic data, we focused on two novel HIV targets with commercially available antibodies: ARID5A and PTPN22. These proteins were readily identified in proteomic datasets from primary T cells (9–14 unique peptides) but not CEM-T4s, and consistently depleted across all donors with a fold change > 2 (***Figure 3D***). As expected, depletion was also seen by immunoblot (***Figure 3E***).

We previously showed that substrates of different HIV accessory proteins could be distinguished by their characteristic patterns of temporal regulation in HIV-infected CEM-T4s (***Greenwood et al., 2016***), and similar clustering was observed in primary T cells (***Figure 2—figure supplement 3A***). Vpr is packaged stoichiometrically in virions (***Cohen et al., 1990***; ***Yu et al., 1990***; ***Yuan et al., 1990***) and, since the number of fusogenic HIV particles exceeds the infectious MOI by at least several fold (***Thomas et al., 2007***), all cells in our time course experiment were necessarily exposed to incoming Vpr. Accordingly, depletion of known Vpr substrates was near-maximal by 24 hr in infected (red, SBP-ΔLNGFR positive) cells, with partial depletion also seen in uninfected (blue, SBP-ΔLNGFR negative) cells (***Figure 2E***, upper panel). In contrast, since de novo viral protein synthesis is absolutely required, depletion of known Vif, Nef and Vpu substrates increased progressively from 24 to 48 hr, and was only seen in HIV-infected (red, SBP-ΔLNGFR positive) cells (***Figure 2E***, lower panel).

Based on their patterns of temporal regulation, ARID5A and PTPN22 are therefore very likely to represent novel Vpr substrates, specific for primary T cells (***Figure 2—figure supplement 3B***). Consistent with this, another member of the ARID5 subfamily of AT-rich interaction domain (ARID)-

containing proteins, ARID5B, is a widely conserved target of Vpr variants from primate lentiviruses (**Greenwood et al., 2019**), and shares a similar temporal profile (**Figure 2—figure supplement 3C**).

Comprehensive analysis of recognised and novel Vif targets in primary T cells

As predicted, both APOBEC3 and PPP2R5 family proteins were depleted in primary CD4+ T cells infected with WT, but not ΔVif viruses (**Figure 5A–B**). Vif-dependent depletion of PPP2R5A-E causes a marked increase in protein phosphorylation in HIV-infected CEM-T4 T cells, particularly substrates of the aurora kinases (AURKA/B) (**Greenwood et al., 2016**). AURKB activity is enhanced by 'activation loop' auto-phosphorylation at threonine 232 (T232), antagonised by PP2A-B56 (**Meppelink et al., 2015**; **Yasui et al., 2004**). Accordingly, a marked increase in AURKB T232 phosphorylation is seen in CEM-T4s transduced with Vif as a single transgene (**Figure 5C**). We therefore confirmed depletion of PPP2R5D by immunoblot of AFMACS-selected primary T cells and, as a functional correlate, observed increased AURKB phosphorylation (**Figure 5D**).

Besides these known substrates, we also noted differential regulation of several other proteins in primary T cells infected with WT vs ΔVif viruses (**Figure 5A**). Modest changes in PPP2R1A, PPP2R1B and PPP2CA (catalytic/structural subunits of the trimeric PP2A holoenzyme) and PPFIA1 and SGO1 (known PP2A interactors) (**Liu et al., 2014**; **Tang et al., 2006**; **Xu et al., 2009**) are likely to be secondary to destabilisation of PP2A by PPP2R5 depletion, or reflect proximity of the holoenzyme to the Vif-cullin E3 ligase complex (**Figure 5B**). Conversely, DPH7 and FMR1 are not known to interact physically with PP2A, and show more profound and consistent depletion (**Figure 5E**). We therefore suspected these proteins to be novel Vif substrates.

To confirm these findings, we first re-examined our proteomic data from CEM-T4s (**Greenwood et al., 2016**). Unlike ARID5A and PTPN22, DPH7 and FMR1 are expressed in CEM-T4 as well as primary T cells, and only decreased in abundance in HIV-infected cells in the presence of Vif (**Figure 5E**). Next, we confirmed Vif-dependent depletion of both proteins by immunoblot, in cells infected with WT (but not ΔVif) viruses (**Figure 5F**). Finally, we repeated these observations in cells transduced with Vif as a single transgene (**Figure 5G**). Vif is therefore both necessary and sufficient for depletion of DPH7 and FMR1 and, taken together with APOBEC3 and PPP2R5 family proteins/interactors, we can account for all significant Vif-dependent changes in the natural target cell of HIV infection.

Discussion

Compared with FACS, bead-based magnetic sorting is fast, simple and scalable for simultaneous processing of multiple samples and large cell numbers (**Plouffe et al., 2015**). In conventional, antibody-based immunomagnetic selection, cells remain coated with beads and antibody-antigen complexes, risking alteration of their behaviour or viability through cross-linking of cell-surface receptors or internalisation of ferrous beads (**Bernard et al., 2002**; **Plouffe et al., 2015**; **Stanciu et al., 1996**). Conversely, AFMACS-based selection is antibody free, and selected cells are released from the beads by incubation with biotin, suitable for a full range of downstream applications (**Matheson et al., 2014**). The HIV-AFMACS virus described in this study allows routine isolation of HIV-infected cells subjected to an MOI $\leq$ 1, avoiding artefacts associated with high MOIs and facilitating experiments in primary cells, where high levels of infection are difficult to achieve in practice.

To demonstrate the utility of this system and provide a resource for the community, we have generated the first high coverage proteomic atlas of HIV-infected primary human CD4+ T cells. As well as identifying HIV-dependent changes in cells from multiple donors, viral regulation may be assessed against a background of endogenous regulation triggered by T cell activation. Unlike T cell lines, primary T cells express a full range of proteins relevant to HIV infection *in vivo*, and are not confounded by the genetic and epigenetic effects of transformation. Furthermore, proteins unique to primary T cells were significantly more likely to be regulated by HIV infection than proteins detected in both primary T cells and CEM-T4s (131/1252 = 10.5% vs 519/7537 = 6.9%; $p < 0.0001$, two-tailed Fisher's exact test). Our data validate many, but not all, previously reported HIV accessory protein targets. For some Vpu/Nef substrates, such as NTB-A and CCR7, downregulation from the plasma membrane may occur in the absence of protein degradation (**Bolduan et al., 2013**; **Ramirez et al., 2014**; **Shah et al., 2010**). For others, such as ICAM-1/3, accessory protein expression may prevent

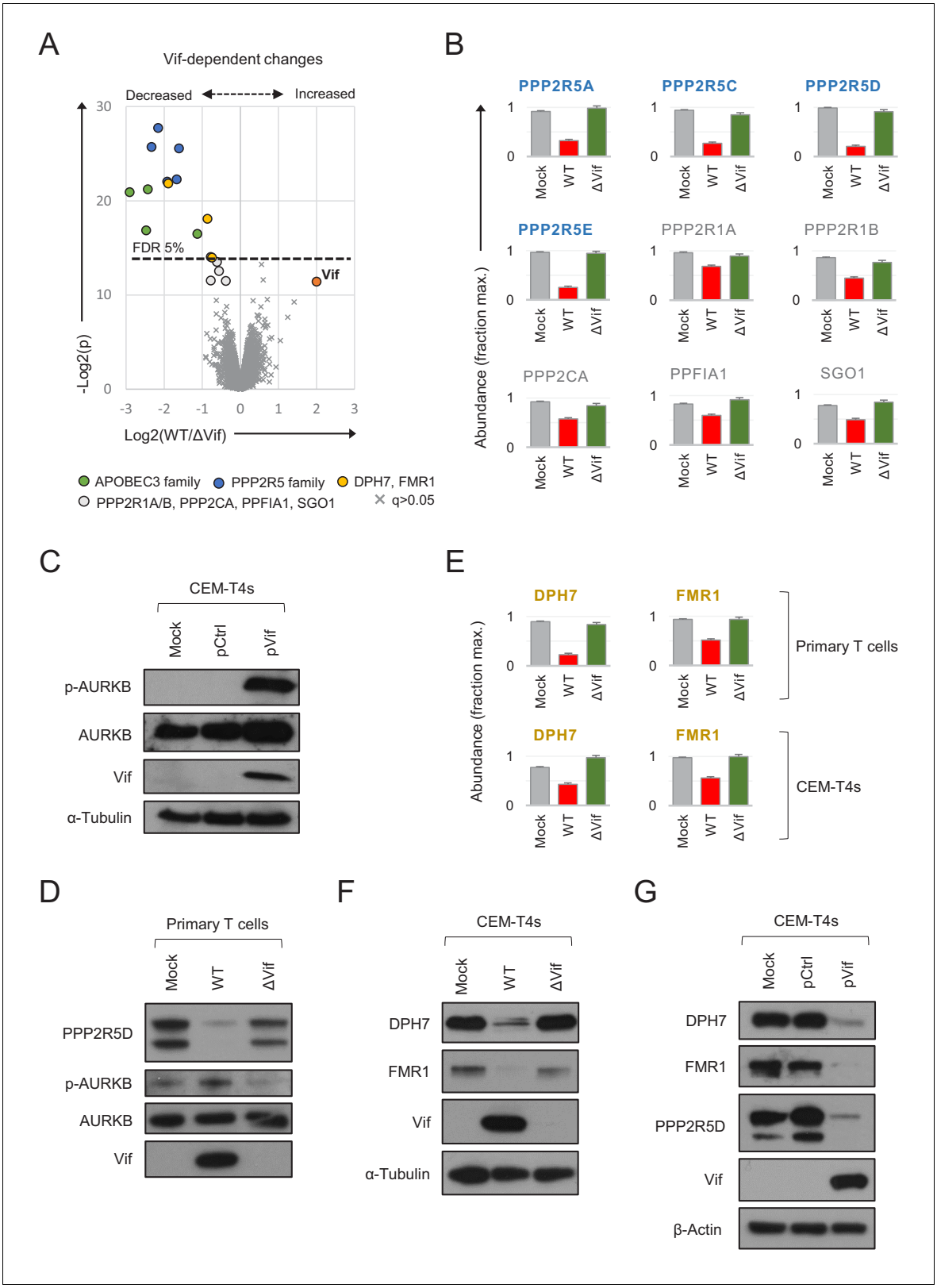

Figure 5. Vif-dependent cellular targets in primary T cells. (**A**) Protein abundances in WT HIV-infected vs ΔVif HIV-infected cells from single time point proteomic experiment (***Figure 3A***). Statistical significance (y axis) vs fold change (x axis) is shown for 8795 cellular and viral proteins quantitated in cells from all three donors (no missing values). Proteins with Benjamini-Hochberg FDR-adjusted p values (q values) < 0.05 or > 0.05 are indicated (FDR threshold of 5%). Highlighted groups of differentially regulated proteins are summarised in the key, including two quantitated isoforms of PP2R5C

Figure 5 continued on next page

Figure 5 continued

(Q13362 and Q13362-4) and FMR1 (Q06787 and Q06787-2). (**B**) Abundances of Vif-dependent PPP2R5 family and related proteins highlighted in **a**) in mock-infected (grey), WT HIV-infected (red) and ΔVif HIV-infected (green) cells from single time point proteomic experiment (***Figure 3A***). Mean abundances (fraction of maximum) with 95% CIs are shown. Only the canonical isoform of PPP2R5C (Q13362) is shown. (**C**) Activation of AURKB by Vif. CEM-T4s were mock-transduced or transduced with control (pCtrl) or Vif-expressing (pVif) lentiviruses for 48 hr (62–78% GFP+), lysed in 2% SDS and analysed by immunoblot with anti-phospho-AURK (T232), anti-total AURKB, anti-Vif and anti-α-tubulin antibodies. (**D**) Vif-dependent activation of AURKB. AFMACS-selected (LNGFR+) HIV-infected cells from ***Figure 3A*** (donor A) were lysed in 2% SDS and analysed by immunoblot with anti-PPP2R5D, anti-phospho-AURK (T232), anti-total AURKB and anti-Vif antibodies. Same lysates as ***Figure 3E***. (**E**) Abundances of DPH7 and FMR1 in mock-infected (grey), WT HIV-infected (red) and ΔVif HIV-infected (green) primary T cells from single time point proteomic experiment (***Figure 3A***) and CEM-T4s (***Greenwood et al., 2016***). Mean abundances (fraction of maximum) with 95% CIs intervals are shown. Only the canonical isoform of FMR1 (Q06787) is shown. (**F**) Vif-dependent depletion of DPH7 and FMR1. CEM-T4s were mock-infected or infected with WT or ΔVif HIV-AFMACS viruses for 48 hr (77–82% LNGFR +cells), lysed in 2% SDS, and analysed by immunoblot with anti-DPH7, ant-FMR1, anti-Vif and anti-α-tubulin antibodies. (**G**) Depletion of DPH7, FMR1 and PPP2R5D by Vif. CEM-T4s were mock-transduced or transduced with control (pCtrl) or Vif-expressing (pVif) lentiviruses for 48 hr (86–88% GFP +cells), lysed in 2% SDS and analysed by immunoblot with anti-phospho-AURK, anti-total AURKB, anti-Vif and anti- α-tubulin (loading control) antibodies.

DOI: https://doi.org/10.7554/eLife.41431.018

upregulation, without reducing levels below baseline (***Sugden et al., 2017***). Alternatively, and particularly where targets have been discovered using model cell line or overexpression systems, regulation may not be quantitatively significant at the protein level in the context and/or natural cell of HIV infection.

Previous temporal proteomic analyses of HIV-infected primary human CD4+ T cells were hampered by extremely limited coverage of the cellular proteome (< 2000 proteins), and did not detect regulation of known or novel HIV accessory protein targets (***Chan et al., 2009***; ***Nemeth et al., 2017***). A more recent study quantitated 7761 proteins in FACS-sorted T cells at a single time point 96 hr post-infection with an R5-tropic, GFP-expressing Nef-deficient virus (***Kuo et al., 2018***). Depletion of several accessory protein targets (including APOBEC3 and PPP2R5 families) was confirmed, and many proteins differentially regulated at 96 hr were also regulated at 48 hr in our study (***Figure 3—figure supplement 5A***). In keeping with the late time point, changes were dominated by pathways involved in cell death and survival, and factors maintaining viability of HIV-infected T cells (such as BIRC5) were enriched. Conversely, the full dataset is not available, effect sizes were generally compressed (***Figure 3—figure supplement 5A***), and 413/650 (64%) of the HIV-dependent changes identified in our study were obscured, including depletion of ARID5A, PTPN22, DPH7 and 19/51 known accessory protein substrates (***Figure 3—figure supplement 5B***).

Compared with other studies, the depth of proteomic coverage reported here not only increases the number of proteins identified, but also reduces the variability in quantitation ('noise'). For example, > 90% of proteins are quantitated using two or more unique peptides. Furthermore, the homogeneous populations of cells analysed (> 90% infected) maximise effect sizes ('signal'), and ensure that proteins exhibiting the most statistically significant differences are also those with the biggest fold changes. Because the 'signal-to-noise ratio' is high, positive controls (known viral targets) behave extremely consistently across our datasets (as shown, for example, in ***Figure 3C*** and ***Figure 2—figure supplement 1B***), and it is possible to make predictions about other cellular proteins falling in the same regions of the volcano plots, and/or exhibiting similar temporal profiles. Our results are therefore useful as a resource (that is, general description of all protein changes), not just as a screen (to identify far outliers).

To enhance viral titers, avoid Env-dependent cytotoxicity, enable synchronous single round infections and bypass co-receptor-dependent targeting of T cell lineages with pre-existing proteomic differences, we used an Env-deficient proviral backbone and pseudotyped viruses with VSVg. Pseudotyping with VSVg redirects HIV viral entry away from the plasma membrane towards an endocytic pathway (***Aiken, 1997***), and may abrogate Env-dependent integrin (***Arthos et al., 2008***) and chemokine co-receptor (***Wu and Yoder, 2009***) signalling early in infection. To limit the impact of these effects, we focussed our analysis on cellular proteins progressively regulated over 48 hr infection. Since only 1/650 HIV-dependent perturbations at this time point was also observed in cells transduced with control lentiviral particles, it is very unlikely that pseudotyping with VSVg per se caused significant artefactual proteomic changes in our datasets (false positives). Nonetheless, it is

possible that the absence of Env-CD4/co-receptor interactions resulted in an underestimate of proteomic changes induced by full length HIV (false negatives), which may vary depending on tropism of the virus (**Wiredja et al., 2018**; **Wojcechowskyj et al., 2013**).

Temporal profiling is particularly well suited to identifying and characterising host factors regulated directly by viral proteins. Because of the need for de novo synthesis of cell surface SBP-Δ LNGFR, it is not possible to perform AFMACS-based selection of HIV-infected primary T cells very early in infection. Nonetheless, even with a first time point 24 hr post-infection, we were able to successfully categorise cellular accessory protein targets according to their patterns of regulation in the time course proteomic experiment. In fact, as we show here, accessory proteins account for much or most of the proteomic remodelling in HIV-infected cells. The abundance of direct accessory protein targets likely explains why proteins and processes/pathways downregulated by HIV in primary T cells correlate so well with changes seen in T cell lines, and are robust to inter-individual variation. In comparison, upregulated proteins concord less well with changes in T cell lines, and functional effects are less homogeneous. This may be because upregulated proteins reflect indirect effects (for example, secondary changes in transcription), which are more likely to be cell-type specific.

Amongst the HIV accessory proteins, Vif was thought until recently to exclusively degrade APOBEC3 family cytidine deaminases. As well as confirming equivalently-potent Vif-dependent depletion of PPP2R5 family phosphatase subunits in primary T cells, our data revealed unexpected Vif-dependent depletion of DPH7 and FMR1. Further work will be required to confirm that these proteins are recruited directly for degradation by the ubiquitin-proteasome system, determine whether (like APOBEC3 and PPP2R5 proteins) they are antagonised by Vif variants from diverse primate and non-primate lentiviral lineages, and identify relevant *in vitro* virological phenotypes associated with target depletion. Nonetheless, FMR1 is already known to reduce HIV virus infectivity when over-expressed in producer cells (**Pan et al., 2009**), and the other novel targets highlighted in this study also impact processes relevant for HIV replication, such as inflammatory cytokine signalling (ARID5A) (**Higa et al., 2018**), T cell activation (PTPN22) (**Hasegawa et al., 2004**) and translational fidelity (DPH7) (**Carette et al., 2009**; **Ortiz et al., 2006**). The diversity of these targets underscores the benefit of an unbiased, systems-level approach to viral infection, and the capacity of the resources presented in this study to reveal unsuspected aspects of the host-virus interaction in the natural target cell of HIV infection.

Materials and methods

Key resources table

Reagent type (species) or resource	Designation	Source or reference	Identifiers	Additional information
Cell line	CEM-T4	NIH AIDS Reagent Program	Cat. #: 117	
Antibody	Mouse monoclonal BV421-conjugated anti-CD4	BioLegend	Cat. #: 317434	Flow cytometry
Antibody	Mouse monoclonal PE-conjugated anti-CD4	BD Biosciences	Cat. #: 561843	Flow cytometry
Antibody	Mouse monoclonal PE-conjugated anti-tetherin	BioLegend	Cat. #: 348405	Flow cytometry
Antibody	Mouse monoclonal AF647-conjugated anti-LNGFR	BioLegend	Cat. #: 345114	Flow cytometry
Antibody	Mouse monoclonal FITC-conjugated anti-LNGFR	BioLegend	Cat. #: 345103	Flow cytometry

Continued on next page

Continued

Reagent type (species) or resource	Designation	Source or reference	Identifiers	Additional information
Antibody	Rabbit monoclonal anti-PPP2R5D	Abcam	Cat. #: ab188323	Immunoblot
Antibody	Mouse monoclonal anti-HIV-1 Vif	NIH AIDS Reagent Program	Cat. #: 6459	Immunoblot
Antibody	Mouse monoclonal anti-p24	Abcam	Cat. #: ab9071	Immunoblot
Antibody	Mouse monoclonal anti-HIV-1 Nef	NIH AIDS Reagent Program	Cat. #: 3689	Immunoblot
Antibody	Rabbit monoclonal anti-PTPN22 (D6D1H)	Cell Signalling Technology	Cat. #: 14693	Immunoblot
Antibody	Mouse monoclonal anti-ARID5A	GeneTex	Cat. #: GTX631940	Immunoblot
Antibody	Rabbit polyclonal anti-FMR1 (FMRP)	Cell Signalling Technology	Cat. #: 4317	Immunoblot
Antibody	Rabbit polyclonal anti-DPH7	Atlas Antibodies	Cat. #: HPA022911	Immunoblot
Antibody	Mouse monoclonal anti-α-tubulin	Cell Signalling Technology	Cat. #: 3873	Immunoblot
Antibody	Mouse monoclonal anti-β-actin	Sigma	Cat. #: A5316	Immunoblot
Antibody	Rabbit polyclonal anti-total AURKB	Cell Signalling Technology	Cat. #: 3094	Immunoblot
Antibody	Rabbit monoclonal anti-phospho-AURK	Cell Signalling Technology	Cat. #: 2914	Immunoblot
Recombinant DNA reagent	HIV-AFMACS	This paper	GenBank: MK435310	pNL4-3-ΔEnv-Nef-P2A-SBP-ΔLNGFR proviral construct (see Materials and methods)
Recombinant DNA reagent	pCtrl	(***Matheson et al., 2014***)	Not applicable	pHRSIN-SE-P2A-SBP-ΔLNGFR-W expression vector
Recombinant DNA reagent	pVif	This paper	Not applicable	pHRSIN-SE-P2A-Vif-hu-W expression vector (see Materials and methods)
Recombinant DNA reagent	pSBP-ΔLNGFR	This paper	Not applicable	pHRSIN-S-P2A-SBP-ΔLNGFR-W expression vector (see Materials and methods)
Recombinant DNA reagent	pTat/SBP-ΔLNGFR	This paper	Not applicable	pLTR-Tat-P2A-SBP-ΔLNGFR expression vector (see Materials and methods)
Commercial assay or kit	Dynabeads Untouched Human CD4 T Cells kit	Invitrogen	Cat. #: 11346D	
Commercial assay or kit	Dynabeads Human T-Activator CD3/CD28	Gibco	Cat. #: 11132D	
Commercial assay or kit	Dynabeads Biotin Binder	Invitrogen	Cat. #: 11047	
Commercial assay or kit	iST-NHS Sample Preparation Kit	PreOmics	Cat. #: P.O.00030	

Continued on next page

Continued

Reagent type (species) or resource	Designation	Source or reference	Identifiers	Additional information
Commercial assay or kit	S-Trap micro MS Sample Preparation Kit	Protifi	Cat. #: C02-micro	
Commercial assay or kit	TMT10plex Isobaric Label Reagent Set	Thermo Scientific	Cat. #: 90110	
Chemical compound, drug	Lympholyte-H	Cedarlane Laboratories	Cat. #: CL5020	
Chemical compound, drug	IL-2	PeproTech	Cat. #: 200–02	Recombinant human IL-2
Chemical compound, drug	Lenti-X Concentrator	Clontech	Cat. #: 631232	
Software, algorithm	Proteome Discoverer 2.1	Thermo Scientific	RRID: SCR_014477	
Software, algorithm	DAVID 6.8	(**Huang et al., 2009a**; **Huang et al., 2009b**)	RRID: SCR_001881	https://david.ncifcrf.gov/
Software, algorithm	Cytoscape 3.6.1	(**Shannon et al., 2003**)	RRID: SCR_003032	http://cytoscape.org/
Software, algorithm	Enrichment Map 3.1.0 Cystoscape plugin	(**Merico et al., 2010**)	RRID: SCR_016052	http://baderlab.org/Software/EnrichmentMap
Software, algorithm	Cluster 3.0	(**de Hoon et al., 2004**)	RRID: SCR_013505	http://bonsai.hgc.jp/~mdehoon/software/cluster/software.htm
Software, algorithm	Java TreeView 1.1.6r4	(**Saldanha, 2004**)	RRID:SCR_013503	http://jtreeview.sourceforge.net

General cell culture

CEM-T4 T cells (CEM-T4s) (**Foley et al., 1965**) were obtained directly (< 1 year) from the AIDS Reagent Program, Division of AIDS, NIAD, NIH: Dr J.P. Jacobs and cultured in RPMI supplemented with 10% FCS, 100units/ml penicillin and 0.1 mg/ml streptomycin at 37°C in 5% CO2. HEK-293T cells were obtained from Lehner laboratory stocks (authenticated by STR profiling [**Menzies et al., 2018**; **Miles et al., 2017**]) and cultured in DMEM supplemented with 10% FCS, 100units/ml penicillin and 0.1 mg/ml streptomycin at 37°C in 5% CO2. All cells were confirmed to be mycoplasma negative (Lonza MycoAlert).

Primary cell isolation and culture

Primary human CD4+ T cells were isolated from peripheral blood by density gradient centrifugation over Lympholyte-H (Cedarlane Laboratories) and negative selection using the Dynabeads Untouched Human CD4 T Cells kit (Invitrogen) according to the manufacturer's instructions. Purity was assessed by flow cytometry for CD3 and CD4 and routinely found to be $\geq$ 95%. Cells were activated using Dynabeads Human T-Activator CD3/CD28 beads (Gibco) according to the manufacturer's instructions and cultured in RPMI supplemented with 10% FCS, 30 U/ml recombinant human IL-2 (PeproTech), 100units/ml penicillin and 0.1 mg/ml streptomycin at 37°C in 5% CO2.

Ethics statement

Ethical permission for this study was granted by the University of Cambridge Human Biology Research Ethics Committee (HBREC.2017.20). Written informed consent was obtained from all volunteers prior to providing blood samples.

HIV-1 molecular clones

pNL4-3-ΔEnv-EGFP (**Zhang et al., 2004**) was obtained from the AIDS Reagent Program, Division of AIDS, NIAD, NIH: Drs Haili Zhang, Yan Zhou, and Robert Siliciano and the complete proviral sequence verified by Sanger sequencing (Source BioScience). Derived from the HIV-1 molecular clone pNL4-3, it encodes EGFP in the *env* ORF), resulting in a large, critical *env* deletion and expression of a truncated Env-EGFP fusion protein retained in the endoplasmic reticulum (ER) by a 3' KDEL ER-retention signal.

The SBP-ΔLNGFR selection marker comprises the high-affinity 38 amino acid SBP fused to the N-terminus of a truncated (non-functional) member of the Tumour Necrosis Factor Receptor superfamily (LNGFR) (**Matheson et al., 2014**). As a type I transmembrane glycoprotein, expression at the cell surface requires a 5' signal peptide.

To replace EGFP with SBP-ΔLNGFR (generating pNL4-3-ΔEnv-SBP-ΔLNGFR) a synthetic gene fragment (gBlock; Integrated DNA Technologies, IDT) was incorporated into pNL4-3-ΔEnv-EGFP by Gibson assembly between SalI/BsaBI sites (gBlock #1; **Supplementary file 1**). In this construct, SBP-ΔLNGFR is fused with the endogenous Env signal peptide.

To express SBP-ΔLNGFR downstream of *nef* and a 'self-cleaving' *Porcine teschovirus-1* 2A (P2A) peptide (generating pNL4-3-ΔEnv-EGFP-Nef-P2A-SBP-ΔLNGFR) a gBlock (IDT) was incorporated into pNL4-3-ΔEnv-EGFP by Gibson assembly between HpaI/XhoI sites (gBlock #2; **Supplementary file 1**). In this construct, SBP-ΔLNGFR is co-translated with codon-optimised Nef (Nef-hu) and includes an exogenous murine immunoglobulin (Ig) signal peptide. SBP-ΔLNGFR was located downstream (rather than upstream) of Nef-hu to avoid disruption of Nef myristoylation by addition of a 5' proline residue following P2A 'cleavage'.

To express SBP-ΔLNGFR downstream of *nef* and an *Encephalomyocarditis virus* (EMCV) internal ribosome entry site (IRES; generating pNL4-3-ΔEnv-EGFP-Nef-IRES-SBP-ΔLNGFR) a gBlock (IDT) was incorporated into pNL4-3-ΔEnv-EGFP by Gibson assembly between HpaI/XhoI sites (gBlock #3; **Supplementary file 1**). In this construct, SBP-ΔLNGFR is translated independently of Nef-hu and includes an exogenous murine Ig signal peptide. A widely-used replication-competent HIV EGFP reporter virus was previously generated using a similar approach (**Schindler et al., 2006**; **Schindler et al., 2003**).

In all constructs, Nef or Nef-hu expression is mediated by the WT HIV LTR promoter and naturally occurring splice sites. In constructs with a P2A peptide or IRES, the use of codon-optimised Nef-hu minimises homology with the U3 region of the 3' LTR (overlapped by the endogenous *nef* sequence) and reduces the risk of recombination.

To remove EGFP from constructs with a P2A peptide or IRES, a gBlock (IDT) was incorporated by Gibson assembly between SalI/BsaBI sites (gBlock #4; **Supplementary file 1**). To avoid generating a truncated protein product fused to the Env signal peptide, the *env* start codon and other potential out of frame start codons in the *vpu* ORF were disrupted with point mutations, whilst maintaining the Vpu protein sequence. Redundant *env* sequence was minimised, without disrupting the Rev response element (RRE).

To truncate the U3 region of the 3' LTR in constructs with a P2A peptide or IRES (with or without EGFP), a gBlock (IDT) was incorporated by Gibson assembly between XhoI/NaeI sites (gBlock #5; **Supplementary file 1**). Previous studies have shown that, in the presence of an intact *nef* ORF, the overlap between *nef* and the U3 region is dispensable for HIV gene expression and replication (**Münch et al., 2005**).

To generate a Vif-deficient HIV-AFMACS molecular clone (pNL4-3-ΔVif-ΔEnv-Nef-P2A-SBP-ΔLNGFR), a restriction fragment encoding a stop codon early in the Vif ORF (after the final in-frame start codon) was subcloned from pNL4-3-ΔVif-ΔEnv-EGFP (**Greenwood et al., 2016**) into pNL4-3-ΔEnv-Nef-P2A-SBP-ΔLNGFR (HIV-AFMACS) between AgeI/PflMI sites.

Where appropriate, additional unique restriction sites were included to facilitate future cloning. All sequences were verified by Sanger sequencing (Source BioScience). The complete HIV-AFMACS sequence is available in **Supplementary file 1**.

Lentivectors for transgene expression

pHRSIN-SE-P2A-SBP-ΔLNGFR-W (referred to as pCtrl in this paper, in which EGFP and SBP-ΔLNGFR expression are mediated by the spleen focus-forming virus (SFFV) promoter and coupled by a P2A peptide) has been previously described (**Matheson et al., 2014**).

For over-expression of SBP-ΔLNGFR as a single transgene, overlapping DNA oligomers (Sigma) encoding a short peptide linker were incorporated into pCtrl in place of EGFP by restriction cloning between BamHI/NotI sites to generate pHRSIN-S-P2A-SBP-ΔLNGFR-W (referred to as pSBP-ΔLNGFR in this paper).

For over-expression of HIV-1 Tat and SBP-ΔLNGFR from the HIV-1 LTR promoter, P2A-SBP-ΔLNGFR was PCR-amplified from HIV-AFMACS and incorporated into pLTR-Tat-IRES-GFP (pEV731, a kind gift from Eric Verdin [**Jordan et al., 2001**]) by Gibson assembly with a bridging gBlock (IDT) between ClaI/XhoI sites. In this construct (pLTR-Tat-P2A-SBP-ΔLNGFR, referred to as pTat/SBP-ΔLNGFR in this paper), Tat and SBP-ΔLNGFR expression are coupled by a P2A peptide, replacing Tat-IRES-GFP in the original lentivector.

For over-expression of codon optimised NL4-3 Vif (Vif-hu), a gBlock (IDT) was incorporated into pCtrl in place of SBP-ΔLNGFR by Gibson assembly between KpnI/XhoI sites to generate pHRSIN-SE-P2A-Vif-hu-W (referred to as pVif in this paper, in which EGFP and Vif-hu expression are coupled by a P2A peptide).

Viral stocks

VSVg-pseudotyped NL4-3-ΔEnv-based viral stocks were generated by co-transfection of HEK-293 T cells with pNL4-3-ΔEnv molecular clones and pMD.G at a ratio of 9:1 (µg) DNA and a DNA:FuGENE 6 ratio of 1 µg:6 µl. Media was changed the next day and viral supernatants harvested and filtered (0.45 µm) at 48 hr prior to concentration with Lenti-X Concentrator (Clontech) and storage at −80°C.

VSVg-pseudotyped lentivector stocks were generated by co-transfection of 293Ts with lentivector, p8.91 and pMD.G at a ratio of 2:1:1 (µg) DNA and a DNA:FuGENE 6 ratio of 1 ug:3 µl. Viral supernatants were harvested, filtered, concentrated and stored as per NL4-3-ΔEnv-based viral stocks.

All viruses and lentivectors were titered by infection/transduction of known numbers of relevant target cells with known volumes of viral stocks under standard experimental conditions, followed by flow cytometry for SBP-ΔLNGFR or EGFP plus/minus CD4 at 48 hr to identify the fraction of infected cells (f) containing at least one transcriptionally active provirus (SBP-ΔLNGFR or EGFP positive plus/minus CD4 low). The number of infectious/transducing units present was then calculated by assuming a Poisson distribution (where $f = 1\text{-}e^{-MOI}$). Typically, a dilution series of each viral stock was tested, and titer determined by linear regression of -ln(1-f) on volume of virus.

T cell infections

CEM-T4s were infected/transduced by spinoculation at 800 g for 2 hr in a non-refrigerated benchtop centrifuge in complete media supplemented with 10 mM HEPES. Primary human CD4+ T cells were infected/transduced using the same protocol 48 hr after activation with CD3/CD28 Dynabeads.

Unlike CEM-T4s, permissivity of infected primary T cells varies between donors/experiments, and the maximum fraction of infected cells in viral dilution series is often around 50% for single round infections, even at high MOI. In practice, we therefore aimed to use sufficient infectious/transducing units to achieve approximately 30% infection, corresponding to a 'nominal' MOI $\leq$ 0.5 (assuming a Poisson distribution). This ensured that, even if only 50% of cells were permissive, the 'effective' MOI would still be $\leq$ 1.

Antibody-Free magnetic cell sorting (AFMACS)

AFMACS-based selection of CEM-T4 or primary human CD4+ T cells using the streptavidin-binding SBP-ΔLNGFR affinity tag was carried out essentially as previously described (**Matheson et al., 2014**). For primary T cells, CD3/CD28 Dynabeads were first removed using a DynaMag-2 magnet (Invitrogen). 24 or 48 hr post-infection, washed cells were resuspended in incubation buffer (IB; Hank's balanced salt solution, 2% dialysed FCS, 1x RPMI Amino Acids Solution (Sigma), 2 mM L-glutamine, 2 mM EDTA and 10 mM HEPES) at 10e7 cells/ml and incubated with Dynabeads Biotin Binder (Invitrogen) at a bead-to-total cell ratio of 4:1 for 30 min at 4°C. Bead-bound cells expressing SBP-ΔLNGFR

were selected using a DynaMag-2 (Invitrogen), washed to remove uninfected cells, then released from the beads by incubation in complete RPMI with 2 mM biotin for 15 min at room temperature (RT). Enrichment was routinely assessed by flow cytometry pre- and post-selection.

Proteomic analysis

Sample preparation

For TMT-based whole cell proteomic analysis of primary human CD4+ T cells, resting or activated cells were washed with ice-cold PBS with Ca/Mg pH 7.4 (Sigma) and frozen at −80°C. Samples were lysed, reduced, alkylated, digested and labelled with TMT reagents (Thermo Scientific) using either iST-NHS (PreOmics GmbH; time course and single time point experiments) or S-Trap (Protifi; SBP-Δ LNGFR control experiment) sample preparation kits, according to the manufacturers' instructions. Typically, 5e6 resting or 1e6 activated cells were used for each condition.

Off-line high pH reversed-phase (HpRP) peptide fractionation

HpRP fractionation was conducted on an Ultimate 3000 UHPLC system (Thermo Scientific) equipped with a 2.1 mm ×15 cm, 1.7 µm Acquity BEH C18 column (Waters, UK). Solvent A was 3% ACN, solvent B was 100% ACN, and solvent C was 200 mM ammonium formate (pH 10). Throughout the analysis C was kept at a constant 10%. The flow rate was 400 µL/min and UV was monitored at 280 nm. Samples were loaded in 90% A for 10 min before a gradient elution of 0–10% B over 10 min (curve 3), 10–34% B over 21 min (curve 5), 34–50% B over 5 min (curve 5) followed by a 10 min wash with 90% B. 15 s (100 µL) fractions were collected throughout the run. Peptide-containing fractions were orthogonally recombined into 24 fractions (e.g. fractions 1, 25, 49, 73 and 97) and dried in a vacuum centrifuge. Fractions were stored at −80°C prior to analysis.

Mass spectrometry

Data were acquired on an Orbitrap Fusion mass spectrometer (Thermo Scientific) coupled to an Ultimate 3000 RSLC nano UHPLC (Thermo Scientific). HpRP fractions were resuspended in 20 µl 5% DMSO 0.5% TFA and 10 uL injected. Fractions were loaded at 10 µl/min for 5 min on to an Acclaim PepMap C18 cartridge trap column (300 um ×5 mm, 5 um particle size) in 0.1% TFA. Solvent A was 0.1% FA and solvent B was ACN/0.1% FA. After loading, a linear gradient of 3–32% B over 3 hr was used for sample separation over a column of the same stationary phase (75 µm × 50 cm, 2 µm particle size) before washing at 90% B and re-equilibration.

An SPS/MS3 acquisition was used for all samples and was run as follows. MS1: Quadrupole isolation, 120'000 resolution, 5e5 AGC target, 50 ms maximum injection time, ions injected for all parallelisable time. MS2: Quadrupole isolation at an isolation width of m/z 0.7, CID fragmentation (NCE 35) with the ion trap scanning out in rapid mode from m/z 120, 8e3 AGC target, 70 ms maximum injection time, ions accumulated for all parallelisable time. In synchronous precursor selection mode the top 10 MS2 ions were selected for HCD fragmentation (65NCE) and scanned out in the orbitrap at 50'000 resolution with an AGC target of 2e4 and a maximum accumulation time of 120 ms, ions were not accumulated for all parallelisable time. The entire MS/MS/MS cycle had a target time of 3 s. Dynamic exclusion was set to ±10 ppm for 90 s, MS2 fragmentation was trigged on precursor ions 5e3 counts and above.

Data processing and analysis

Spectra were searched by Mascot within Proteome Discoverer 2.1 in two rounds. The first search was against the UniProt Human reference proteome (26/09/17), the HIV-AFMACS proteome and compendium of common contaminants (GPM). The second search took all unmatched spectra from the first search and searched against the human trEMBL database (Uniprot, 26/09/17). For time course and single time point experiments, the following search parameters were used. MS1 Tol: 10 ppm. MS2 Tol: 0.6 Da. Fixed Mods: Ist-alkylation (+113.084064 Da) (C) and TMT (N-term, K). Var Mods: Oxidation (M). Enzyme: Trypsin (/P). For the SBP-ΔLNGFR control experiment, Carbamidomethyl (C) modification was used in place of Ist-Alkylation. MS3 spectra were used for reporter ion-based quantitation with a most confident centroid tolerance of 20 ppm. Peptide spectrum match (PSM) false discovery rate (FDR) was calculated using Mascot percolator and was controlled at 0.01% for 'high' confidence PSMs and 0.05% for 'medium' confidence PSMs. Normalisation was

automated and based on total s/n in each channel. Proteins/peptides satisfying at least a 'medium' FDR confidence were taken forth to statistical analysis in R. This consisted of a moderated T-test (Limma) with Benjamini-Hochberg correction for multiple hypotheses to provide a q value for each comparison (**Schwämmle et al., 2013**). Further data manipulation and general statistical analysis (including principal component analysis) was conducted using Excel, XLSTAT and GraphPad Prism 7.

All mass spectrometry proteomics data from this study have been deposited to the ProteomeXchange Consortium via the PRIDE (**Vizcaíno et al., 2016**) partner repository with the dataset identifier PXD012263 and 10.6019/PXD012263 (accessible at http://proteomecentral.proteomexchange.org).

For functional analysis of proteins significantly downregulated or upregulated by WT HIV ($q < 0.05$) in the single time point proteomic experiment (**Figure 3A**), enrichment of Gene Ontology (GO) Biological Process (GOTERM_BP_FAT) and Molecular Function (GOTERM_MF_FAT) terms against a background of all proteins quantitated was determined using the Database for Annotation, Visualization and Integrated Discovery (DAVID) 6.8 (accessed on 22/7/2018 at https://david.ncifcrf.gov/) with default settings (**Huang et al., 2009a**; **Huang et al., 2009b**). Human proteins annotated to GO:0016126 (sterol biosynthetic process) were retrieved from AmiGO 2 (accessed on 27/7/2018 at http://amigo.geneontology.org/amigo) (**Carbon et al., 2009**). To account for redundancy between annotations, enriched GO terms were visualised using the Enrichment Map 3.1.0 plugin (**Merico et al., 2010**) for Cytoscape 3.6.1. (downloaded from http://cytoscape.org/) (**Shannon et al., 2003**) with default settings (q value cut-off of 0.1) and sparse-intermediate connectivity. Clusters were manually labelled to highlight the prevalent biological functions amongst each set of related annotations.

For clustering according to profiles of temporal expression, known accessory protein substrates from **Figure 2C–D** and **Figure 2—figure supplement 1B** and additional Vpr substrates shown in **Figure 3C** were analysed using Cluster 3.0 (downloaded from http://bonsai.hgc.jp/~mdehoon/software/cluster/software.htm) (**de Hoon et al., 2004**) and visualised using Java TreeView 1.1.6r4 (downloaded from http://jtreeview.sourceforge.net) (**Saldanha, 2004**). Only proteins significantly downregulated by WT HIV ($q < 0.05$) in the single time point proteomic experiment (**Figure 3A**) were included. Where more than one isoform was quantitated, only the canonical isoform was used (PPP2R5C, Q13362; ZGPAT, Q8N5A5; NUSAP1, Q9BXS6). Data from the time course proteomic experiment (**Figure 2A**) were expressed as log2(ratio)s of abundances in experimental (Expt):control (Ctrl) cells for each condition/time point, and range-scaled to highlight patterns of temporal expression relative to the biological response range (minimum-maximum) for each protein. Agglomerative hierarchical clustering was performed using uncentered Pearson correlation and centroid linkage (**Eisen et al., 1998**).

Comparison with CEM-T4 T cells

To compare results between primary and transformed T cells at a similar depth of proteomic coverage, we re-analysed TMT-labelled peptide eluates from a previous study (**Greenwood et al., 2016**) conducted in CEM-T4s spinoculated in triplicate with VSVg-pseudotyped NL4-3-ΔEnv-EGFP WT or ΔVif viruses at an MOI of 1.5. This extended analysis consisted of reinjection of HpRP fractions on longer (3 hr) gradients using a higher performance (75 as opposed to 50 cm) analytical column and the MS parameters employed in this study. In total, the new CEM-T4 dataset covered 8065 proteins, comparable with the datasets from primary T cells described here.

Comparisons with other published datasets

A previous study quantitated 7816 proteins at multiple time points following *in vitro* activation of naïve (CD45RA+ CCR7+) primary human CD4+ human T cells with plate-bound anti-CD23 and anti-CD28 antibodies (**Geiger et al., 2016**). For comparison with this study, a filtered list of 5907 proteins quantitated in at least two samples from both resting cells and cells activated for 48 hr was used.

We have recently characterised 34 new Vpr substrates, together with further, extensive Vpr-dependent changes (downregulated and upregulated proteins) in HIV-infected CEM-T4s (**Greenwood et al., 2019**). For comparison with this study, a list of 1388 proteins concordantly regulated by Vpr ($q < 0.05$) in the context of both viral infection and Vpr-bearing virus-like particles was compiled from the published datasets.

RUNX1 target genes were previously found to be regulated by Vif at a transcriptional level because of competition for CBFβ binding (**Kim et al., 2013**). For comparison with this study, the reported list of 155 genes with RUNX1-associated regulatory domains exhibiting Vif-dependent differential gene expression in Jurkat T cells after 4 or 6 hr of PMA and PHA treatment was used.

Curated lists of ISGs have been previously described (**Schoggins et al., 2014**; **Schoggins et al., 2011**). For comparison with this study, a list of 377 ISGs was compiled from these studies.

A recent study quantitated 7761 proteins in FACS-sorted T cells at a single time point 96 hr post-infection with an R5-tropic, GFP-expressing Nef-deficient virus (**Kuo et al., 2018**). The comparator is GFP negative rather than mock-infected cells (equivalent to SBP-ΔLNGFR negative cells in this study), and the full dataset is not available. For comparison with this study, the published list of 1551 differentially expressed proteins ($q < 0.05$) was therefore used.

Flow cytometry

For primary T cells, CD3/CD28 Dynabeads were first removed using a DynaMag-2 magnet (Invitrogen). Typically 2e5 washed cells were incubated for 15 min in 100 µL PBS with the indicated fluorochrome-conjugated antibody. All steps were performed on ice or at 4˚C and stained cells were fixed in PBS/1% paraformaldehyde.

Immunoblotting

Cells were lysed in PBS/2% SDS supplemented with Halt Protease Inhibitor Cocktail (Thermo Scientific) and Halt Phosphatase Inhibitor Cocktail (Thermo Scientific) for 10 min at RT. Benzonase (Sigma) was included to reduce lysate viscosity. Post-nuclear supernatants were heated in Laemelli Loading Buffer for 25 min at 50˚C, separated by SDS-PAGE and transferred to Immobilon-P membrane (Millipore). Membranes were blocked in PBS/5% non-fat dried milk (Marvel)/0.2% Tween and probed with the indicated primary antibody overnight at 4˚C. Reactive bands were visualised using HRP-conjugated secondary antibodies and SuperSignal West Pico or Dura chemiluminescent substrates (Thermo Scientific). Typically 10–20 µg total protein was loaded per lane (Pierce BCA Protein Assay kit).

Antibodies

Antibodies for immunoblot and flow cytometry are detailed in the Key resources table. The following antibodies were obtained from the AIDS Reagent Program, Division of AIDS, NIAID, NIH: mouse monoclonal anti-HIV-1 Vif (**Simon et al., 1995**) from Dr MH Malim, and mouse monoclonal anti-HIV-1 Nef (**Chang et al., 1998**) from Dr JA Hoxie.

Acknowledgements

This work was supported by the MRC (CSF MR/P008801/1 to NJM), NHSBT (WPA15-02 to NJM), the Wellcome Trust (PRF 210688/Z/18/Z to PJL), the NIHR Cambridge BRC, and a Wellcome Trust Strategic Award to CIMR. The authors thank Dr Reiner Schulte and the CIMR Flow Cytometry Core Facility team, and members of the Lehner laboratory for critical discussion.

Additional information

Funding

Funder	Grant reference number	Author
Medical Research Council	MR/P008801/1	Nicholas J Matheson
NHS Blood and Transplant	WPA15-02	Nicholas J Matheson
Wellcome	210688/Z/18/Z	Paul J Lehner

The funders had no role in study design, data collection and interpretation, or the decision to submit the work for publication.

Author contributions

Adi Naamati, Conceptualization, Formal analysis, Validation, Investigation, Visualization, Methodology, Writing—original draft, Writing—review and editing; James C Williamson, Data curation, Formal analysis, Supervision, Investigation, Methodology, Writing—review and editing; Edward JD Greenwood, Conceptualization, Investigation, Writing—review and editing; Sara Marelli, Conceptualization, Validation, Investigation, Writing—review and editing; Paul J Lehner, Conceptualization, Resources, Supervision, Funding acquisition, Project administration, Writing—review and editing; Nicholas J Matheson, Conceptualization, Resources, Data curation, Formal analysis, Supervision, Funding acquisition, Visualization, Methodology, Writing—original draft, Project administration, Writing—review and editing

Author ORCIDs

Edward JD Greenwood http://orcid.org/0000-0002-5224-0263
Paul J Lehner http://orcid.org/0000-0001-9383-1054
Nicholas J Matheson https://orcid.org/0000-0002-3318-1851

Ethics

Human subjects: Ethical permission for this study was granted by the University of Cambridge Human Biology Research Ethics Committee (HBREC.2017.20). Written informed consent was obtained from all volunteers prior to providing blood samples.

Decision letter and Author response

Decision letter https://doi.org/10.7554/eLife.41431.025
Author response https://doi.org/10.7554/eLife.41431.026

Additional files

Supplementary files

- Supplementary file 1. gBlock and HIV-AFMACS sequences.

DOI: https://doi.org/10.7554/eLife.41431.019

- Transparent reporting form

DOI: https://doi.org/10.7554/eLife.41431.020

Data availability

All data generated or analysed during this study are included in the manuscript and supporting files. Source data files have been provided for Figures 2 and 3. All mass spectrometry proteomics data have been deposited to the ProteomeXchange Consortium via the PRIDE partner repository with the dataset identifier PXD012263 and 10.6019/PXD012263 (accessible at http://proteomecentral.proteomexchange.org).

The following dataset was generated:

Author(s)	Year	Dataset title	Dataset URL	Database and Identifier
Naamati A, Williamson JC, Greenwood EJD, Marelli S	2018	Functional proteomic atlas of HIV infection in primary human CD4+ T cells	http://proteomecentral.proteomexchange.org/cgi/GetDataset?ID=PXD012263	ProteomeXchange Consortium , PXD012263

References

Aiken C. 1997. Pseudotyping human immunodeficiency virus type 1 (HIV-1) by the glycoprotein of vesicular stomatitis virus targets HIV-1 entry to an endocytic pathway and suppresses both the requirement for nef and the sensitivity to cyclosporin A. *Journal of Virology* **71**:5871–5877. PMID: 9223476

Apps R, Del Prete GQ, Chatterjee P, Lara A, Brumme ZL, Brockman MA, Neil S, Pickering S, Schneider DK, Piechocka-Trocha A, Walker BD, Thomas R, Shaw GM, Hahn BH, Keele BF, Lifson JD, Carrington M. 2016. HIV-1 vpu mediates HLA-C downregulation. *Cell Host & Microbe* **19**:686–695. DOI: https://doi.org/10.1016/j.chom.2016.04.005, PMID: 27173934

Arthos J, Cicala C, Martinelli E, Macleod K, Van Ryk D, Wei D, Xiao Z, Veenstra TD, Conrad TP, Lempicki RA, McLaughlin S, Pascuccio M, Gopaul R, McNally J, Cruz CC, Censoplano N, Chung E, Reitano KN, Kottilil S, Goode DJ, et al. 2008. HIV-1 envelope protein binds to and signals through integrin alpha4beta7, the gut mucosal homing receptor for peripheral T cells. *Nature Immunology* **9**:301–309. DOI: https://doi.org/10.1038/ni1566, PMID: 18264102

Bernard F, Jaleco S, Dardalhon V, Steinberg M, Yssel H, Noraz N, Taylor N, Kinet S. 2002. Ex vivo isolation protocols differentially affect the phenotype of human CD4+ T cells. *Journal of Immunological Methods* **271**: 99–106. DOI: https://doi.org/10.1016/S0022-1759(02)00412-X, PMID: 12445733

Bolduan S, Hubel P, Reif T, Lodermeyer V, Höhne K, Fritz JV, Sauter D, Kirchhoff F, Fackler OT, Schindler M, Schubert U. 2013. HIV-1 vpu affects the anterograde transport and the glycosylation pattern of NTB-A. *Virology* **440**:190–203. DOI: https://doi.org/10.1016/j.virol.2013.02.021, PMID: 23528733

Bolduan S, Reif T, Schindler M, Schubert U. 2014. HIV-1 vpu mediated downregulation of CD155 requires alanine residues 10, 14 and 18 of the transmembrane domain. *Virology* **464**:375–384. DOI: https://doi.org/10.1016/j.virol.2014.07.034, PMID: 25113908

Carbon S, Ireland A, Mungall CJ, Shu S, Marshall B, Lewis S AmiGO Hub Web Presence Working Group. 2009. AmiGO: online access to ontology and annotation data . *Bioinformatics* **25**:288–289. DOI: https://doi.org/10.1093/bioinformatics/btn615, PMID: 19033274

Carette JE, Guimaraes CP, Varadarajan M, Park AS, Wuethrich I, Godarova A, Kotecki M, Cochran BH, Spooner E, Ploegh HL, Brummelkamp TR. 2009. Haploid genetic screens in human cells identify host factors used by pathogens. *Science* **326**:1231–1235. DOI: https://doi.org/10.1126/science.1178955, PMID: 19965467

Chan EY, Sutton JN, Jacobs JM, Bondarenko A, Smith RD, Katze MG. 2009. Dynamic host energetics and cytoskeletal proteomes in human immunodeficiency virus type 1-infected human primary CD4 cells: analysis by multiplexed label-free mass spectrometry. *Journal of Virology* **83**:9283–9295. DOI: https://doi.org/10.1128/JVI.00814-09, PMID: 19587052

Chang AH, Hoxie JA, Cassol S, O'Shaughnessy M, Jirik F. 1998. Construction of single-chain antibodies that bind an overlapping epitope of HIV-1 nef. *FEBS Letters* **441**:307–312. DOI: https://doi.org/10.1016/S0014-5793(98)01569-5, PMID: 9883905

Cohen EA, Dehni G, Sodroski JG, Haseltine WA. 1990. Human immunodeficiency virus vpr product is a virion-associated regulatory protein. *Journal of Virology* **64**:3097–3099. PMID: 2139896

Cohen GB, Gandhi RT, Davis DM, Mandelboim O, Chen BK, Strominger JL, Baltimore D. 1999. The selective downregulation of class I major histocompatibility complex proteins by HIV-1 protects HIV-infected cells from NK cells. *Immunity* **10**:661–671. DOI: https://doi.org/10.1016/S1074-7613(00)80065-5, PMID: 10403641

de Hoon MJ, Imoto S, Nolan J, Miyano S. 2004. Open source clustering software. *Bioinformatics* **20**:1453–1454. DOI: https://doi.org/10.1093/bioinformatics/bth078, PMID: 14871861

Eisen MB, Spellman PT, Brown PO, Botstein D. 1998. Cluster analysis and display of genome-wide expression patterns. *PNAS* **95**:14863–14868. DOI: https://doi.org/10.1073/pnas.95.25.14863, PMID: 9843981

Foley GE, Handler AH, Lynch PM, Wolman SR, Stulberg CS, Eagle H. 1965. Loss of neoplastic properties in vitro. II. observations on KB sublines. *Cancer Research* **25**:1254–1261. PMID: 5839717

Geiger R, Rieckmann JC, Wolf T, Basso C, Feng Y, Fuhrer T, Kogadeeva M, Picotti P, Meissner F, Mann M, Zamboni N, Sallusto F, Lanzavecchia A. 2016. L-Arginine modulates T cell metabolism and enhances survival and Anti-tumor activity. *Cell* **167**:829–842. DOI: https://doi.org/10.1016/j.cell.2016.09.031

Gheysen D, Jacobs E, de Foresta F, Thiriart C, Francotte M, Thines D, De Wilde M. 1989. Assembly and release of HIV-1 precursor Pr55gag virus-like particles from recombinant baculovirus-infected insect cells. *Cell* **59**:103–112. DOI: https://doi.org/10.1016/0092-8674(89)90873-8, PMID: 2676191

Gillet JP, Varma S, Gottesman MM. 2013. The clinical relevance of cancer cell lines. *JNCI Journal of the National Cancer Institute* **105**:452–458. DOI: https://doi.org/10.1093/jnci/djt007, PMID: 23434901

Goujon C, Moncorgé O, Bauby H, Doyle T, Ward CC, Schaller T, Hué S, Barclay WS, Schulz R, Malim MH. 2013. Human MX2 is an interferon-induced post-entry inhibitor of HIV-1 infection. *Nature* **502**:559–562. DOI: https://doi.org/10.1038/nature12542, PMID: 24048477

Greenwood EJ, Matheson NJ, Wals K, van den Boomen DJ, Antrobus R, Williamson JC, Lehner PJ. 2016. Temporal proteomic analysis of HIV infection reveals remodelling of the host phosphoproteome by lentiviral vif variants. *eLife* **5**:e18296. DOI: https://doi.org/10.7554/eLife.18296, PMID: 27690223

Greenwood EJ, Williamson JC, Sienkiewicz A, Naamati A, Matheson NJ, Lehner PJ. 2019. Promiscuous targeting of cellular proteins by Vpr drives massive proteomic remodelling in HIV-1 infection. *bioRxiv*. DOI: https://doi.org/10.1101/364067

Guy B, Kieny MP, Riviere Y, Le Peuch C, Dott K, Girard M, Montagnier L, Lecocq JP. 1987. HIV F/3' orf encodes a phosphorylated GTP-binding protein resembling an oncogene product. *Nature* **330**:266–269. DOI: https://doi.org/10.1038/330266a0, PMID: 3118220

Haller C, Müller B, Fritz JV, Lamas-Murua M, Stolp B, Pujol FM, Keppler OT, Fackler OT. 2014. HIV-1 nef and vpu are functionally redundant broad-spectrum modulators of cell surface receptors, including tetraspanins. *Journal of Virology* **88**:14241–14257. DOI: https://doi.org/10.1128/JVI.02333-14, PMID: 25275127

Harris RS, Bishop KN, Sheehy AM, Craig HM, Petersen-Mahrt SK, Watt IN, Neuberger MS, Malim MH. 2003. DNA deamination mediates innate immunity to retroviral infection. *Cell* **113**:803–809. DOI: https://doi.org/10.1016/S0092-8674(03)00423-9, PMID: 12809610

Hasegawa K, Martin F, Huang G, Tumas D, Diehl L, Chan AC. 2004. PEST domain-enriched tyrosine phosphatase (PEP) regulation of effector/memory T cells. *Science* **303**:685–689. DOI: https://doi.org/10.1126/science.1092138, PMID: 14752163

He J, Choe S, Walker R, Di Marzio P, Morgan DO, Landau NR. 1995. Human immunodeficiency virus type 1 viral protein R (Vpr) arrests cells in the G2 phase of the cell cycle by inhibiting p34cdc2 activity. *Journal of Virology* **69**:6705–6711. PMID: 7474080

Higa M, Oka M, Fujihara Y, Masuda K, Yoneda Y, Kishimoto T. 2018. Regulation of inflammatory responses by dynamic subcellular localization of RNA-binding protein Arid5a. *PNAS* **115**:E1214–E1220. DOI: https://doi.org/10.1073/pnas.1719921115, PMID: 29358370

Hrecka K, Hao C, Gierszewska M, Swanson SK, Kesik-Brodacka M, Srivastava S, Florens L, Washburn MP, Skowronski J. 2011. Vpx relieves inhibition of HIV-1 infection of macrophages mediated by the SAMHD1 protein. *Nature* **474**:658–661. DOI: https://doi.org/10.1038/nature10195, PMID: 21720370

Hrecka K, Hao C, Shun MC, Kaur S, Swanson SK, Florens L, Washburn MP, Skowronski J. 2016. HIV-1 and HIV-2 exhibit divergent interactions with HLTF and UNG2 DNA repair proteins. *PNAS* **113**:E3921–E3930. DOI: https://doi.org/10.1073/pnas.1605023113, PMID: 27335459

Huang daW, Sherman BT, Lempicki RA. 2009a. Bioinformatics enrichment tools: paths toward the comprehensive functional analysis of large gene lists. *Nucleic Acids Research* **37**:1–13. DOI: https://doi.org/10.1093/nar/gkn923, PMID: 19033363

Huang daW, Sherman BT, Lempicki RA. 2009b. Systematic and integrative analysis of large gene lists using DAVID bioinformatics resources. *Nature Protocols* **4**:44–57. DOI: https://doi.org/10.1038/nprot.2008.211, PMID: 19131956

Jain P, Boso G, Langer S, Soonthornvacharin S, De Jesus PD, Nguyen Q, Olivieri KC, Portillo AJ, Yoh SM, Pache L, Chanda SK. 2018. Large-Scale arrayed analysis of protein degradation reveals cellular targets for HIV-1 vpu. *Cell Reports* **22**:2493–2503. DOI: https://doi.org/10.1016/j.celrep.2018.01.091, PMID: 29490283

Jordan A, Defechereux P, Verdin E. 2001. The site of HIV-1 integration in the human genome determines basal transcriptional activity and response to tat transactivation. *The EMBO Journal* **20**:1726–1738. DOI: https://doi.org/10.1093/emboj/20.7.1726, PMID: 11285236

Jowett JB, Planelles V, Poon B, Shah NP, Chen ML, Chen IS. 1995. The human immunodeficiency virus type 1 vpr gene arrests infected T cells in the G2 + M phase of the cell cycle. *Journal of Virology* **69**:6304–6313. PMID: 7666531

Karn J, Stoltzfus CM. 2012. Transcriptional and posttranscriptional regulation of HIV-1 gene expression. *Cold Spring Harbor Perspectives in Medicine* **2**:a006916. DOI: https://doi.org/10.1101/cshperspect.a006916, PMID: 22355797

Keefe AD, Wilson DS, Seelig B, Szostak JW. 2001. One-step purification of recombinant proteins using a nanomolar-affinity streptavidin-binding peptide, the SBP-Tag. *Protein Expression and Purification* **23**:440–446. DOI: https://doi.org/10.1006/prep.2001.1515, PMID: 11722181

Kim DY, Kwon E, Hartley PD, Crosby DC, Mann S, Krogan NJ, Gross JD. 2013. Cbfβ stabilizes HIV vif to counteract APOBEC3 at the expense of RUNX1 target gene expression. *Molecular Cell* **49**:632–644. DOI: https://doi.org/10.1016/j.molcel.2012.12.012, PMID: 23333304

Klotman ME, Kim S, Buchbinder A, DeRossi A, Baltimore D, Wong-Staal F. 1991. Kinetics of expression of multiply spliced RNA in early human immunodeficiency virus type 1 infection of lymphocytes and monocytes. *PNAS* **88**:5011–5015. DOI: https://doi.org/10.1073/pnas.88.11.5011, PMID: 1711215

Kumar M, Keller B, Makalou N, Sutton RE. 2001. Systematic determination of the packaging limit of lentiviral vectors. *Human Gene Therapy* **12**:1893–1905. DOI: https://doi.org/10.1089/104303401753153947, PMID: 11589831

Kuo H-H, Ahmad R, Lee GQ, Gao C, Chen H-R, Ouyang Z, Szucs MJ, Kim D, Tsibris A, Chun T-W, Battivelli E, Verdin E, Rosenberg ES, Carr SA, Yu XG, Lichterfeld M. 2018. Anti-apoptotic protein BIRC5 maintains survival of HIV-1-Infected $CD4^+$ T cells. *Immunity* **48**:1183–1194. DOI: https://doi.org/10.1016/j.immuni.2018.04.004

Laguette N, Sobhian B, Casartelli N, Ringeard M, Chable-Bessia C, Ségéral E, Yatim A, Emiliani S, Schwartz O, Benkirane M. 2011. SAMHD1 is the dendritic- and myeloid-cell-specific HIV-1 restriction factor counteracted by vpx. *Nature* **474**:654–657. DOI: https://doi.org/10.1038/nature10117, PMID: 21613998

Laguette N, Brégnard C, Hue P, Basbous J, Yatim A, Larroque M, Kirchhoff F, Constantinou A, Sobhian B, Benkirane M. 2014. Premature activation of the SLX4 complex by vpr promotes G2/M arrest and escape from innate immune sensing. *Cell* **156**:134–145. DOI: https://doi.org/10.1016/j.cell.2013.12.011, PMID: 24412650

Lahouassa H, Blondot ML, Chauveau L, Chougui G, Morel M, Leduc M, Guillonneau F, Ramirez BC, Schwartz O, Margottin-Goguet F. 2016. HIV-1 vpr degrades the HLTF DNA translocase in T cells and macrophages. *PNAS* **113**:5311–5316. DOI: https://doi.org/10.1073/pnas.1600485113, PMID: 27114546

Lambelé M, Koppensteiner H, Symeonides M, Roy NH, Chan J, Schindler M, Thali M. 2015. Vpu is the main determinant for tetraspanin downregulation in HIV-1-infected cells. *Journal of Virology* **89**:3247–3255. DOI: https://doi.org/10.1128/JVI.03719-14, PMID: 25568205

Lapek JD, Lewinski MK, Wozniak JM, Guatelli J, Gonzalez DJ. 2017. Quantitative temporal viromics of an inducible HIV-1 model yields insight to global host targets and Phospho-Dynamics associated with protein vpr. *Molecular & Cellular Proteomics* **16**:1447–1461. DOI: https://doi.org/10.1074/mcp.M116.066019

Lim ES, Fregoso OI, McCoy CO, Matsen FA, Malik HS, Emerman M. 2012. The ability of primate lentiviruses to degrade the monocyte restriction factor SAMHD1 preceded the birth of the viral accessory protein vpx. *Cell Host & Microbe* **11**:194–204. DOI: https://doi.org/10.1016/j.chom.2012.01.004, PMID: 22284954

Liu YC, Couzens AL, Deshwar AR, B McBroom-Cerajewski LD, Zhang X, Puviindran V, Scott IC, Gingras AC, Hui CC, Angers S. 2014. The PPFIA1-PP2A protein complex promotes trafficking of Kif7 to the ciliary tip and hedgehog signaling. *Science Signaling* **7**:ra117. DOI: https://doi.org/10.1126/scisignal.2005608, PMID: 25492966

Lv L, Wang Q, Xu Y, Tsao L-C, Nakagawa T, Guo H, Su L, Xiong Y. 2018. Vpr targets TET2 for degradation by CRL4 VprBP E3 ligase to sustain IL-6 expression and enhance HIV-1 replication. *Molecular Cell* **70**:961–970. DOI: https://doi.org/10.1016/j.molcel.2018.05.007

Matheson NJ, Peden AA, Lehner PJ. 2014. Antibody-free magnetic cell sorting of genetically modified primary human CD4+ T cells by one-step streptavidin affinity purification. *PLoS ONE* **9**:e111437. DOI: https://doi.org/10.1371/journal.pone.0111437, PMID: 25360777

Matheson NJ, Sumner J, Wals K, Rapiteanu R, Weekes MP, Vigan R, Weinelt J, Schindler M, Antrobus R, Costa AS, Frezza C, Clish CB, Neil SJ, Lehner PJ. 2015. Cell surface proteomic map of HIV infection reveals antagonism of amino acid metabolism by vpu and nef. *Cell Host & Microbe* **18**:409–423. DOI: https://doi.org/10.1016/j.chom.2015.09.003, PMID: 26439863

Matusali G, Potestà M, Santoni A, Cerboni C, Doria M. 2012. The human immunodeficiency virus type 1 nef and vpu proteins downregulate the natural killer cell-activating ligand PVR. *Journal of Virology* **86**:4496–4504. DOI: https://doi.org/10.1128/JVI.05788-11, PMID: 22301152

Maudet C, Sourisce A, Dragin L, Lahouassa H, Rain JC, Bouaziz S, Ramirez BC, Margottin-Goguet F. 2013. HIV-1 Vpr induces the degradation of ZIP and sZIP, adaptors of the NuRD chromatin remodeling complex, by hijacking DCAF1/VprBP. *PLoS ONE* **8**:e77320. DOI: https://doi.org/10.1371/journal.pone.0077320, PMID: 24116224

Menzies SA, Volkmar N, van den Boomen DJ, Timms RT, Dickson AS, Nathan JA, Lehner PJ. 2018. The sterol-responsive RNF145 E3 ubiquitin ligase mediates the degradation of HMG-CoA reductase together with gp78 and Hrd1. *eLife* **7**:e40009. DOI: https://doi.org/10.7554/eLife.40009, PMID: 30543180

Meppelink A, Kabeche L, Vromans MJ, Compton DA, Lens SM. 2015. Shugoshin-1 balances aurora B kinase activity via PP2A to promote chromosome bi-orientation. *Cell Reports* **11**:508–515. DOI: https://doi.org/10.1016/j.celrep.2015.03.052, PMID: 25892238

Merico D, Isserlin R, Stueker O, Emili A, Bader GD. 2010. Enrichment map: a network-based method for gene-set enrichment visualization and interpretation. *PLoS ONE* **5**:e13984. DOI: https://doi.org/10.1371/journal.pone.0013984, PMID: 21085593

Miles AL, Burr SP, Grice GL, Nathan JA. 2017. The vacuolar-ATPase complex and assembly factors, TMEM199 and CCDC115, control HIF1α prolyl hydroxylation by regulating cellular iron levels. *eLife* **6**:e22693. DOI: https://doi.org/10.7554/eLife.22693, PMID: 28296633

Münch J, Rajan D, Rücker E, Wildum S, Adam N, Kirchhoff F. 2005. The role of upstream U3 sequences in HIV-1 replication and CD4+ T cell depletion in human lymphoid tissue ex vivo. *Virology* **341**:313–320. DOI: https://doi.org/10.1016/j.virol.2005.07.023, PMID: 16102792

Neil SJ, Zang T, Bieniasz PD. 2008. Tetherin inhibits retrovirus release and is antagonized by HIV-1 vpu. *Nature* **451**:425–430. DOI: https://doi.org/10.1038/nature06553, PMID: 18200009

Nemeth J, Vongrad V, Metzner KJ, Strouvelle VP, Weber R, Pedrioli P, Aebersold R, Günthard HF, Collins BC. 2017. In vivo and in vitro Proteome Analysis of Human Immunodeficiency Virus (HIV)-1-infected, Human $CD4^+$ T Cells. *Molecular & Cellular Proteomics* **16**:S108–S123. DOI: https://doi.org/10.1074/mcp.M116.065235, PMID: 28223351

O'Doherty U, Swiggard WJ, Malim MH. 2000. Human immunodeficiency virus type 1 spinoculation enhances infection through virus binding. *Journal of Virology* **74**:10074–10080. DOI: https://doi.org/10.1128/JVI.74.21.10074-10080.2000, PMID: 11024136

Ortiz PA, Ulloque R, Kihara GK, Zheng H, Kinzy TG. 2006. Translation elongation factor 2 anticodon mimicry domain mutants affect fidelity and diphtheria toxin resistance. *Journal of Biological Chemistry* **281**:32639–32648. DOI: https://doi.org/10.1074/jbc.M607076200, PMID: 16950777

Pan Q, Rong L, Zhao X, Liang C. 2009. Fragile X mental retardation protein restricts replication of human immunodeficiency virus type 1. *Virology* **387**:127–135. DOI: https://doi.org/10.1016/j.virol.2009.02.006, PMID: 19249802

Plouffe BD, Murthy SK, Lewis LH. 2015. Fundamentals and application of magnetic particles in cell isolation and enrichment: a review. *Reports on Progress in Physics* **78**:016601. DOI: https://doi.org/10.1088/0034-4885/78/1/016601, PMID: 25471081

Poon B, Jowett JB, Stewart SA, Armstrong RW, Rishton GM, Chen IS. 1997. Human immunodeficiency virus type 1 vpr gene induces phenotypic effects similar to those of the DNA alkylating agent, nitrogen mustard. *Journal of Virology* **71**:3961–3971. PMID: 9094673

Popovic M, Read-Connole E, Gallo R. 1984. T4 positive human neoplastic cell lines susceptible to and permissive for htlv-iii. *The Lancet* **324**:1472–1473. DOI: https://doi.org/10.1016/S0140-6736(84)91666-0

Ramirez PW, Famiglietti M, Sowrirajan B, DePaula-Silva AB, Rodesch C, Barker E, Bosque A, Planelles V. 2014. Downmodulation of CCR7 by HIV-1 vpu results in impaired migration and chemotactic signaling within $CD4^+$ T cells. *Cell Reports* **7**:2019–2030. DOI: https://doi.org/10.1016/j.celrep.2014.05.015, PMID: 24910430

Re F, Braaten D, Franke EK, Luban J. 1995. Human immunodeficiency virus type 1 vpr arrests the cell cycle in G2 by inhibiting the activation of p34cdc2-cyclin B. *Journal of Virology* **69**:6859–6864. PMID: 7474100

Rogel ME, Wu LI, Emerman M. 1995. The human immunodeficiency virus type 1 vpr gene prevents cell proliferation during chronic infection. *Journal of Virology* **69**:882–888. PMID: 7815556

Romani B, Shaykh Baygloo N, Aghasadeghi MR, Allahbakhshi E. 2015. HIV-1 vpr protein enhances proteasomal degradation of MCM10 DNA replication factor through the Cul4-DDB1[VprBP] E3 ubiquitin ligase to induce G2/M cell cycle arrest. *Journal of Biological Chemistry* **290**:17380–17389. DOI: https://doi.org/10.1074/jbc.M115.641522, PMID: 26032416

Rosa A, Chande A, Ziglio S, De Sanctis, Bertorelli R, Goh SL, McCauley SM, Nowosielska A, Antonarakis SE, Luban J, Santoni FA, Pizzato M. 2015. HIV-1 nef promotes infection by excluding SERINC5 from virion incorporation. *Nature* **526**:212–217. DOI: https://doi.org/10.1038/nature15399, PMID: 26416734

Roshal M, Kim B, Zhu Y, Nghiem P, Planelles V. 2003. Activation of the ATR-mediated DNA damage response by the HIV-1 viral protein R. *Journal of Biological Chemistry* **278**:25879–25886. DOI: https://doi.org/10.1074/jbc.M303948200, PMID: 12738771

Ruggieri L, Aiuti A, Salomoni M, Zappone E, Ferrari G, Bordignon C. 1997. Cell-surface marking of CD(34+)-restricted phenotypes of human hematopoietic progenitor cells by retrovirus-mediated gene transfer. *Human Gene Therapy* **8**:1611–1623. DOI: https://doi.org/10.1089/hum.1997.8.13-1611, PMID: 9322094

Saldanha AJ. 2004. Java treeview–extensible visualization of microarray data. *Bioinformatics* **20**:3246–3248. DOI: https://doi.org/10.1093/bioinformatics/bth349, PMID: 15180930

Schindler M, Würfl S, Benaroch P, Greenough TC, Daniels R, Easterbrook P, Brenner M, Münch J, Kirchhoff F. 2003. Down-modulation of mature major histocompatibility complex class II and up-regulation of invariant chain cell surface expression are well-conserved functions of human and simian immunodeficiency virus nef alleles. *Journal of Virology* **77**:10548–10556. DOI: https://doi.org/10.1128/JVI.77.19.10548-10556.2003, PMID: 12970439

Schindler M, Münch J, Kutsch O, Li H, Santiago ML, Bibollet-Ruche F, Müller-Trutwin MC, Novembre FJ, Peeters M, Courgnaud V, Bailes E, Roques P, Sodora DL, Silvestri G, Sharp PM, Hahn BH, Kirchhoff F. 2006. Nef-mediated suppression of T cell activation was lost in a lentiviral lineage that gave rise to HIV-1. *Cell* **125**:1055–1067. DOI: https://doi.org/10.1016/j.cell.2006.04.033, PMID: 16777597

Schoggins JW, Wilson SJ, Panis M, Murphy MY, Jones CT, Bieniasz P, Rice CM. 2011. A diverse range of gene products are effectors of the type I interferon antiviral response. *Nature* **472**:481–485. DOI: https://doi.org/10.1038/nature09907, PMID: 21478870

Schoggins JW, MacDuff DA, Imanaka N, Gainey MD, Shrestha B, Eitson JL, Mar KB, Richardson RB, Ratushny AV, Litvak V, Dabelic R, Manicassamy B, Aitchison JD, Aderem A, Elliott RM, García-Sastre A, Racaniello V, Snijder EJ, Yokoyama WM, Diamond MS, et al. 2014. Pan-viral specificity of IFN-induced genes reveals new roles for cGAS in innate immunity. *Nature* **505**:691–695. DOI: https://doi.org/10.1038/nature12862, PMID: 24284630

Schröfelbauer B, Yu Q, Zeitlin SG, Landau NR. 2005. Human immunodeficiency virus type 1 vpr induces the degradation of the UNG and SMUG uracil-DNA glycosylases. *Journal of Virology* **79**:10978–10987. DOI: https://doi.org/10.1128/JVI.79.17.10978-10987.2005, PMID: 16103149

Schwämmle V, León IR, Jensen ON. 2013. Assessment and improvement of statistical tools for comparative proteomics analysis of sparse data sets with few experimental replicates. *Journal of Proteome Research* **12**:3874–3883. DOI: https://doi.org/10.1021/pr400045u, PMID: 23875961

Schwartz O, Maréchal V, Le Gall S, Lemonnier F, Heard JM. 1996. Endocytosis of major histocompatibility complex class I molecules is induced by the HIV-1 nef protein. *Nature Medicine* **2**:338–342. DOI: https://doi.org/10.1038/nm0396-338, PMID: 8612235

Shah AH, Sowrirajan B, Davis ZB, Ward JP, Campbell EM, Planelles V, Barker E. 2010. Degranulation of natural killer cells following interaction with HIV-1-infected cells is hindered by downmodulation of NTB-A by vpu. *Cell Host & Microbe* **8**:397–409. DOI: https://doi.org/10.1016/j.chom.2010.10.008, PMID: 21075351

Shannon P, Markiel A, Ozier O, Baliga NS, Wang JT, Ramage D, Amin N, Schwikowski B, Ideker T. 2003. Cytoscape: a software environment for integrated models of biomolecular interaction networks. *Genome Research* **13**:2498–2504. DOI: https://doi.org/10.1101/gr.1239303, PMID: 14597658

Sheehy AM, Gaddis NC, Choi JD, Malim MH. 2002. Isolation of a human gene that inhibits HIV-1 infection and is suppressed by the viral vif protein. *Nature* **418**:646–650. DOI: https://doi.org/10.1038/nature00939, PMID: 12167863

Shrivastava S, Trivedi J, Mitra D. 2016. Gene expression profiling reveals nef induced deregulation of lipid metabolism in HIV-1 infected T cells. *Biochemical and Biophysical Research Communications* **472**:169–174. DOI: https://doi.org/10.1016/j.bbrc.2016.02.089, PMID: 26915805

Simon JH, Southerling TE, Peterson JC, Meyer BE, Malim MH. 1995. Complementation of vif-defective human immunodeficiency virus type 1 by primate, but not nonprimate, lentivirus vif genes. *Journal of Virology* **69**:4166–4172. PMID: 7769676

Stanciu LA, Shute J, Holgate ST, Djukanović R. 1996. Production of IL-8 and IL-4 by positively and negatively selected CD4+ and CD8+ human T cells following a four-step cell separation method including magnetic cell sorting (MACS). *Journal of Immunological Methods* **189**:107–115. DOI: https://doi.org/10.1016/0022-1759(95)00240-5, PMID: 8576572

Sugden SM, Pham TN, Cohen ÉA. 2017. HIV-1 vpu downmodulates ICAM-1 expression, resulting in decreased killing of infected $CD4^+$ T Cells by NK Cells. *Journal of Virology* **91**:e02442. DOI: https://doi.org/10.1128/JVI.02442-16, PMID: 28148794

Tang Z, Shu H, Qi W, Mahmood NA, Mumby MC, Yu H. 2006. PP2A is required for centromeric localization of Sgo1 and proper chromosome segregation. *Developmental Cell* **10**:575–585. DOI: https://doi.org/10.1016/j.devcel.2006.03.010, PMID: 16580887

Thomas JA, Ott DE, Gorelick RJ. 2007. Efficiency of human immunodeficiency virus type 1 postentry infection processes: evidence against disproportionate numbers of defective virions. *Journal of Virology* **81**:4367–4370. DOI: https://doi.org/10.1128/JVI.02357-06, PMID: 17267494

Usami Y, Wu Y, Göttlinger HG. 2015. SERINC3 and SERINC5 restrict HIV-1 infectivity and are counteracted by nef. *Nature* **526**:218–223. DOI: https://doi.org/10.1038/nature15400, PMID: 26416733

van 't Wout AB, Swain JV, Schindler M, Rao U, Pathmajeyan MS, Mullins JI, Kirchhoff F. 2005. Nef induces multiple genes involved in cholesterol synthesis and uptake in human immunodeficiency virus type 1-infected T cells. *Journal of Virology* **79**:10053–10058. DOI: https://doi.org/10.1128/JVI.79.15.10053-10058.2005, PMID: 16014965

Vassena L, Giuliani E, Matusali G, Cohen ÉA, Doria M. 2013. The human immunodeficiency virus type 1 vpr protein upregulates PVR via activation of the ATR-mediated DNA damage response pathway. *Journal of General Virology* **94**:2664–2669. DOI: https://doi.org/10.1099/vir.0.055541-0, PMID: 24045107

Vermeire J, Roesch F, Sauter D, Rua R, Hotter D, Van Nuffel A, Vanderstraeten H, Naessens E, Iannucci V, Landi A, Witkowski W, Baeyens A, Kirchhoff F, Verhasselt B. 2016. HIV triggers a cGAS-Dependent, vpu- and Vpr-Regulated type I interferon response in CD4$^+$ T Cells. *Cell Reports* **17**:413–424. DOI: https://doi.org/10.1016/j.celrep.2016.09.023, PMID: 27705790

Vizcaíno JA, Csordas A, Del-Toro N, Dianes JA, Griss J, Lavidas I, Mayer G, Perez-Riverol Y, Reisinger F, Ternent T, Xu QW, Wang R, Hermjakob H. 2016. 2016 update of the PRIDE database and its related tools. *Nucleic Acids Research* **44**:11033. DOI: https://doi.org/10.1093/nar/gkw880, PMID: 27683222

Weekes MP, Tomasec P, Huttlin EL, Fielding CA, Nusinow D, Stanton RJ, Wang EC, Aicheler R, Murrell I, Wilkinson GW, Lehner PJ, Gygi SP. 2014. Quantitative temporal viromics: an approach to investigate host-pathogen interaction. *Cell* **157**:1460–1472. DOI: https://doi.org/10.1016/j.cell.2014.04.028, PMID: 24906157

Willey RL, Maldarelli F, Martin MA, Strebel K. 1992. Human immunodeficiency virus type 1 vpu protein induces rapid degradation of CD4. *Journal of Virology* **66**:7193–7200. PMID: 1433512

Wiredja DD, Tabler CO, Schlatzer DM, Li M, Chance MR, Tilton JC. 2018. Global phosphoproteomics of CCR5-tropic HIV-1 signaling reveals reprogramming of cellular protein production pathways and identifies p70-S6K1 and MK2 as HIV-responsive kinases required for optimal infection of CD4+ T cells. *Retrovirology* **15**:44. DOI: https://doi.org/10.1186/s12977-018-0423-4, PMID: 29970186

Wojcechowskyj JA, Didigu CA, Lee JY, Parrish NF, Sinha R, Hahn BH, Bushman FD, Jensen ST, Seeholzer SH, Doms RW. 2013. Quantitative phosphoproteomics reveals extensive cellular reprogramming during HIV-1 entry. *Cell Host & Microbe* **13**:613–623. DOI: https://doi.org/10.1016/j.chom.2013.04.011, PMID: 23684312

Wu Y, Yoder A. 2009. Chemokine coreceptor signaling in HIV-1 infection and pathogenesis. *PLoS Pathogens* **5**: e1000520. DOI: https://doi.org/10.1371/journal.ppat.1000520, PMID: 20041213

Xu Z, Cetin B, Anger M, Cho US, Helmhart W, Nasmyth K, Xu W. 2009. Structure and function of the PP2A-shugoshin interaction. *Molecular Cell* **35**:426–441. DOI: https://doi.org/10.1016/j.molcel.2009.06.031, PMID: 19716788

Yasui Y, Urano T, Kawajiri A, Nagata K, Tatsuka M, Saya H, Furukawa K, Takahashi T, Izawa I, Inagaki M. 2004. Autophosphorylation of a newly identified site of Aurora-B is indispensable for cytokinesis. *Journal of Biological Chemistry* **279**:12997–13003. DOI: https://doi.org/10.1074/jbc.M311128200, PMID: 14722118

Ye CJ, Feng T, Kwon HK, Raj T, Wilson MT, Asinovski N, McCabe C, Lee MH, Frohlich I, Paik HI, Zaitlen N, Hacohen N, Stranger B, De Jager P, Mathis D, Regev A, Benoist C. 2014. Intersection of population variation and autoimmunity genetics in human T cell activation. *Science* **345**:1254665. DOI: https://doi.org/10.1126/science.1254665, PMID: 25214635

Yu XF, Matsuda M, Essex M, Lee TH. 1990. Open reading frame vpr of simian immunodeficiency virus encodes a virion-associated protein. *Journal of Virology* **64**:5688–5693. PMID: 2145446

Yuan X, Matsuda Z, Matsuda M, Essex M, Lee TH. 1990. Human immunodeficiency virus vpr gene encodes a virion-associated protein. *AIDS Research and Human Retroviruses* **6**:1265–1271. DOI: https://doi.org/10.1089/aid.1990.6.1265, PMID: 2150318

Zhang H, Zhou Y, Alcock C, Kiefer T, Monie D, Siliciano J, Li Q, Pham P, Cofrancesco J, Persaud D, Siliciano RF. 2004. Novel single-cell-level phenotypic assay for residual drug susceptibility and reduced replication capacity of drug-resistant human immunodeficiency virus type 1. *Journal of Virology* **78**:1718–1729. DOI: https://doi.org/10.1128/JVI.78.4.1718-1729.2004, PMID: 14747537

Zhou X, DeLucia M, Ahn J. 2016. SLX4-SLX1 Protein-independent Down-regulation of MUS81-EME1 protein by HIV-1 viral protein R (Vpr). *Journal of Biological Chemistry* **291**:16936–16947. DOI: https://doi.org/10.1074/jbc.M116.721183, PMID: 27354282